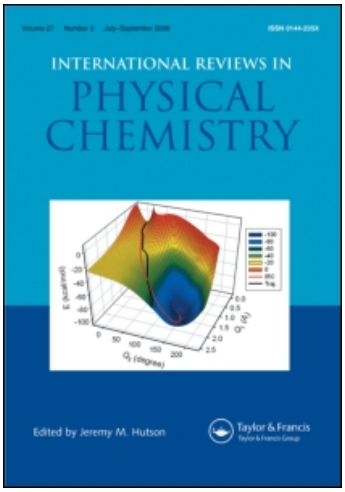

International Reviews in Physical Chemistry
Publication details, including instructions for authors and subscription information:
http://www.informaworld.com/smpp/title~content=t713724383

Microwave spectroscopy of ternary and quaternary van der Waals clusters

Yunjie Xu[a]; Jennifer Van Wijngaarden[b]; Wolfgang Jäger[a]
[a] Department of Chemistry, University of Alberta, Edmonton, AB, Canada T6G 2G2 [b] Department of Chemistry, Mount Holyoke College, South Hadley, MA 01075, USA

To cite this Article Xu, Yunjie , Van Wijngaarden, Jennifer and Jäger, Wolfgang(2005) 'Microwave spectroscopy of ternary and quaternary van der Waals clusters', International Reviews in Physical Chemistry, 24: 2, 301 — 338
To link to this Article: DOI: 10.1080/01442350500252039
URL: http://dx.doi.org/10.1080/01442350500252039

International Reviews in Physical Chemistry,
Vol. 24, No. 2, April–June 2005, 301–338

Taylor & Francis
Taylor & Francis Group

Microwave spectroscopy of ternary and quaternary van der Waals clusters

YUNJIE XU*†, JENNIFER VAN WIJNGAARDEN‡
and WOLFGANG JÄGER*†

†Department of Chemistry, University of Alberta, Edmonton, AB, Canada T6G 2G2
‡Department of Chemistry, Mount Holyoke College, South Hadley, MA 01075, USA

(*Received 9 June 2005; in final form 6 July 2005*)

The study of weakly bound complexes and clusters promises to provide a bridge between the properties of isolated molecules and those of dense phases. We describe briefly the method of pulsed nozzle Fourier transform microwave spectroscopy, which we use in our laboratory to study rotational and low-lying van der Waals vibrational spectra of weakly bound complexes and clusters. Systematic studies of three different classes of clusters are described: (i) mixed rare gas dimers, trimers, and tetramers, where the transition dipole moment is entirely provided by the weak van der Waals interactions; (ii) $(\text{rare gas})_{1,2,3}$–ammonia clusters where the internal motions of the ammonia subunit are affected by the rare gas atom solvation; (iii) $(\text{helium})_{1,2,3}$–molecule clusters, which provide a basis for the study of larger helium atoms containing clusters. We also discuss the effect of three-body non-additive contributions on spectroscopic parameters, such as dipole moments, rotational constants, and nuclear quadrupole coupling constants.

Contents

*Corresponding authors. Email: yunjie.xu@ualberta.ca; wolfgang.jaeger@ualberta.ca

International Reviews in Physical Chemistry
ISSN 0144–235X print/ISSN 1366–591X online
http://www.tandf.co.uk/journals
DOI: 10.1080/01442350500252039

1. Introduction

Spectroscopic studies of van der Waals clusters promise to provide a link between the properties of dense atomic or molecular phases of matter and the properties of the constituent atoms and molecules. One essential prerequisite for building such a link is the availability of binary interaction potentials with high accuracy. Although the necessary binary interaction potentials can in principle be extracted from bulk phase measurements and from collision data, this has in practice been achieved successfully only for the simplest systems [1]. In the past two decades or so, high resolution spectroscopy of binary van der Waals complexes has produced fruitful results for the characterization of intermolecular interactions between two binding partners [2]. Novick's compilation of weakly bound molecular systems that have been investigated spectroscopically or theoretically provides a valuable reference source [3]. Experimental results, often from microwave rotational and infrared ro-vibrational spectroscopy [2], have stimulated theoretical modelling of the binary interactions. For small systems, *ab initio* potential energy surfaces of almost spectroscopic accuracy can now be calculated. Progress in this area was recently reviewed by Tao [4]. In addition, a number of bound state calculation packages have been developed to enable the extraction of eigenstate energies and wavefunctions from potential energy surfaces; see, for example [5–9]. This allows one to evaluate and gauge the quality of the surfaces against experimental spectroscopic data. The intimate connection between potential energy surfaces and spectra of weakly bound complexes has recently been reviewed by Wormer and van der Avoird [10]. Methods have also been developed to improve the accuracy of potential energy surfaces; these range from simple scaling procedures to the more involved morphing approach [11, 12] to reproduce the experimental data. The availability of binary interaction potentials with very high accuracy is a prerequisite for detection of three-body non-additive interactions in the spectroscopic data of larger clusters.

With the accurate binary interaction potential at hand, dense phase properties can be evaluated in terms of those of the constituent atoms and molecules by assuming, in a first approximation, pairwise additivity and by averaging over the relevant orientations and separations. However, to obtain good agreement with the experimental results, three- and more-body non-additive contributions need to be considered as corrections to the pairwise additive approach for the interpretation of bulk phase properties. For example, unambiguous evidence for the importance of three-body non-additive interactions for the properties of condensed phases was found in the crystal structures of solid rare gases [13]. For atomic systems, the Axilrod–Teller triple–dipole term was developed in the early 1960s to account for three-body interactions [14]. The extraction of these non-additive terms from bulk phase measurements is inherently difficult because of the simultaneous presence of three-, four-, and more-body terms.

The ability to study complexes and clusters of specific sizes with high resolution spectroscopic methods allows one, in principle, to isolate the effects of three-, four-, and more-body non-additive contributions. This means one can record and analyse a particular ternary or a quaternary molecular cluster without the interference of any higher order clusters. The technique of pulsed molecular beam Fourier transform microwave spectroscopy is being used for the investigations of rotational spectra of

weakly bound complexes and clusters [15]. A number of ternary and quaternary clusters have been studied with this technique, as detailed below. It is the combination of very high resolution capability and high sensitivity that makes this instrument applicable to the studies of larger clusters. In particular, the ability to resolve lines that are only a few kHz apart is of great advantage for the study of larger, heavier clusters with relatively small rotational constants. It would be increasingly difficult to resolve the transitions for such systems in an infrared spectrum where the linewidth is several hundred times larger than in the microwave region. Microwave spectroscopy allows also the resolution of very narrow hyperfine structures, such as those due to nuclear quadrupole coupling or spin rotation interactions. These hyperfine patterns are often extremely useful in identifying the spectroscopic assignments and provide additional information about the structures and dynamics of the molecular systems. These hyperfine patterns may also supply crucial information about the three-body or more-body interactions as will be discussed below.

The process to quantify the three-body non-additive contributions is highly non-trivial. It requires very accurate binary interaction potentials from which a pairwise additive potential can be constructed. Next, the bound state information has to be extracted from these pairwise additive potentials for comparison with experiment. The difference between the experimental data and those predicted from the pairwise additive potentials is then attributed to three-body non-additive interactions. The pairwise additive potentials can subsequently be modified by including the various three-body terms until satisfactory agreement with experiment is achieved. In practice, this procedure has, for example, been successfully applied to the Ar_2–HCl and Ar_2–HF trimers by Ernesti and Hutson [16], by reproducing the vibrational frequency shifts. This work was subsequently extended to clusters of the type Ar_N–HF ($N = 2, 3, 4, 12$) [17].

The remainder of this review is organized as follows. The experimental techniques used in our laboratory to study rotational and low-lying van der Waals ro-vibrational transitions of weakly bound complexes and clusters are described in section 2. In section 3, we will discuss a number of molecular systems to illustrate various aspects of the spectroscopy of weakly bound complexes and clusters. Concluding remarks are given in section 4.

2. Experimental details

The instrument used for the studies described below is a Fourier transform microwave spectrometer of the Balle–Flygare design [18]. Several similar instruments have been described before; see, for example [19–21]. A schematic diagram of the set-up of our spectrometer [22] is given in figure 1. The sample cell is a microwave Fabry–Perot cavity that consists of two spherical aluminium mirrors with 24 cm radius of curvature and 30 cm diameter. The mirror separation is approximately 30 cm and can be fine-tuned by translating one of the mirrors with a DC MotorMike drive. The cavity is mounted in a vacuum chamber that is pumped by a 12-inch diffusion pump backed by a two-stage rotary pump.

The complexes and clusters are generated in a pulsed molecular expansion through a General Valve, Series 9, nozzle, with a circular nozzle orifice (diameter = 0.8 mm). The

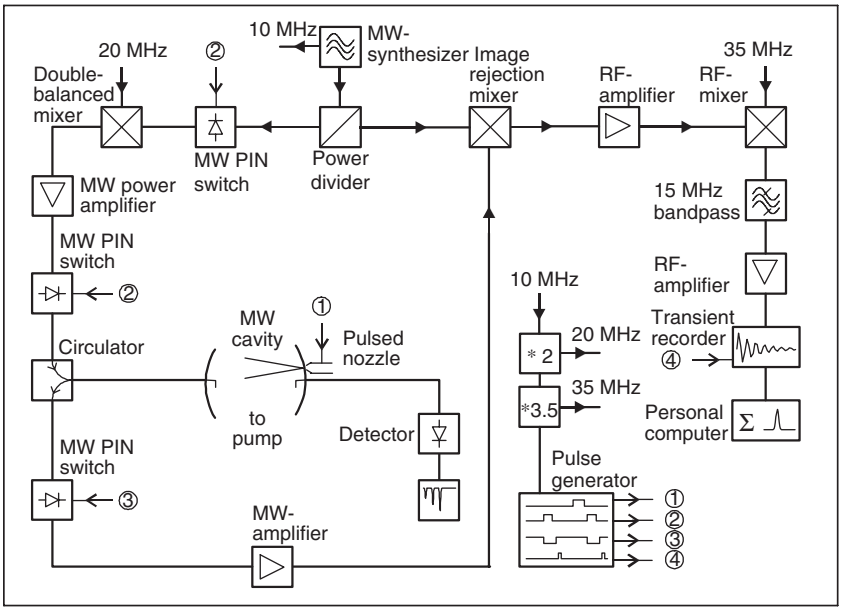

Figure 1. Schematic diagram of the microwave and radio-frequency set-up of the Fourier transform microwave spectrometer.

nozzle is mounted near the centre of the stationary mirror, such that the molecular expansion travels parallel to the cavity axis [18, 23]. The nozzle body is directly accessible and can be cooled if necessary. The parallel arrangement results in a longer time-of-flight of the complexes in the cavity compared to a perpendicular set-up. The longer observation time leads, in turn, to higher sensitivity and increased resolution. Typical linewidths (full-width at half-height) are 7 kHz if neon is used as backing gas and 14–20 kHz for helium. A further consequence of the parallel nozzle arrangement is the splitting of all transitions into two Doppler components. The repetition rate of the experiment is on the order of 2 Hz, limited by the capacity of the diffusion pump. Typical sample mixtures contain 1% or less of the binding partner(s) in neon or helium backing gas at pressures from 1 to 15 atm for the clusters studied.

The experimental technique is based on the pulsed excitation of the molecular sample and subsequent detection of the emission signal. A microwave synthesizer is used as the radiation source. Two microwave PIN diode switches shape the microwave pulse after a power divider. The double balanced mixer generates sidebands at 20 MHz from the carrier frequency. For the investigation of species with small dipole moments, a microwave power amplifier is inserted into the excitation pulse arm of the microwave circuit. The microwave pulse goes through a circulator to a wire-hook antenna and into the microwave cavity. Prior to this, the microwave cavity has been tuned into resonance with the external microwave radiation by moving one of the mirrors with the DC MotorMike drive and monitoring the cavity throughput. A microwave switch protects the detection circuit from the relatively high power excitation pulse. The subsequent molecular emission signal is directed through the circulator into the detection arm

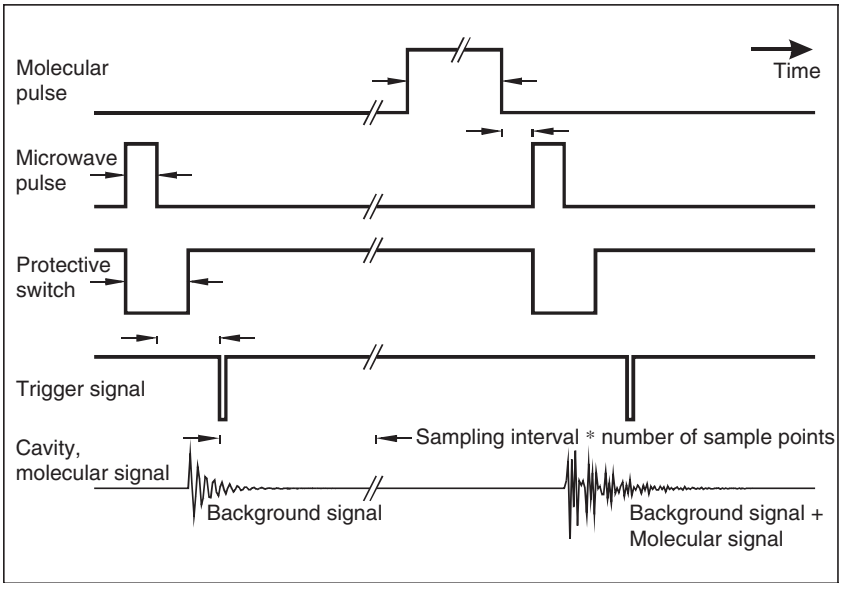

Figure 2. Timing diagram of a pulsed excitation–emission microwave experiment.

of the microwave circuit. The signal is amplified by a low-noise microwave amplifier and converted into the radio-frequency range in two steps. In the first step, the signal is mixed with the original microwave frequency from the synthesizer to frequencies around 20 MHz; in the second step, the signal is mixed to frequencies around 15 MHz. The time domain signal is then digitized and recorded using a PC-based transient recorder card and further processed in the computer. The operating range of our spectrometer is from ~3 to ~26 GHz.

A timing diagram of an individual experiment is given in figure 2. It is essential that all timing and reference signals are phase synchronized to the lowest common subharmonic to ensure in-phase co-addition of the time-domain signals for signal-to-noise improvement. The experiment begins with the application of a microwave excitation pulse into the empty cavity to record a background signal. The excitation pulse length depends on the microwave power and the transition dipole moment and is typically on the order of a few μs. During this time, the protective microwave switch in the detection arm is set to high attenuation. After a sufficient delay time (typically 10–20 μs) to allow the cavity ringing after the excitation to dampen out, the protective switch is opened and a trigger signal is sent to the transient recorder. This pulse sequence is then repeated after a molecular pulse has been injected into the cavity to record the molecular emission signal. The background signal is subtracted and the whole sequence can be repeated several thousand times for signal averaging. With our current set-up, we sample the signal at a rate of 100 MHz and record 8 k data points, resulting in an overall recording time of about 80 μs. The frequency spectrum is obtained after a 16 k Fourier transformation, using 8 k zero-filling for resolution enhancement. This results in 8 k complex data points in the frequency domain over a range of 50 MHz, corresponding to a spacing of 6.1 kHz

between adjacent points in the frequency domain. We usually display the power spectrum and use an interpolation procedure to determine peak frequencies.

It is worthwhile to very briefly describe the technique of pulsed excitation and subsequent recording of the molecular emission signal to provide an explanation for some of the interesting features of Fourier transform microwave spectroscopy. Application of the density matrix formalism to a two-level system that can interact with electromagnetic radiation leads to the electric dipole analogue of the Bloch equations [24, 25] that are well-known for the description of nuclear magnetic resonance spectroscopy. In this description, the application of a near resonant $\pi/2$ microwave excitation pulse reduces the initial population difference between the two levels to zero and puts each molecular system into a superposition state that involves the two stationary state wavefunctions. In addition, the microwave excitation pulse imprints its coherence property onto the molecular sample, such that the superposition states of the individual systems oscillate in phase with each other with the transition frequency. The initial population difference has been 'converted' into a macroscopic dipole moment, i.e. a polarization of the sample. The oscillating molecular dipole moments couple now, in a classical description, to the electromagnetic field and emit radiation with the transition frequency. The signal is a spontaneous emission signal and is observable because of the coherence of the emitters. In this case, the signal is proportional to the square of the number of emitters rather than just to the number of emitters in the incoherent case. The optimal length of the excitation pulse is given by a quarter-cycle ($\pi/2$ pulse) of the so-called Rabi frequency, which, in turn, is proportional to both the transition dipole moment and power of the microwave pulse. For molecular systems with small dipole moments, we therefore use a microwave power amplifier to boost the excitation pulse power to approximately 1 W. This keeps the excitation pulse length below about 10 μs which corresponds to an excitation bandwidth of 100 kHz.

Microwave spectroscopy is an inherently less sensitive technique compared to, for example, infrared or visible spectroscopy. The main reasons are the small population differences between energy levels and the low energy microwave photons that need to be detected. In general, the signal strength goes with the power of two or three of the transition frequency. The great advantage of pulsed nozzle cavity Fourier transform microwave spectroscopy, compared to optical spectroscopy, is the large spatial overlap between microwave beam in the cavity and the unskimmed molecular expansion. This allows a large number of molecular systems to be interrogated simultaneously. The low temperatures of less than 1 K achieved in the molecular expansion increase the sensitivity further for transitions with small rotational quantum number J. An additional advantage for the study of molecular systems with small dipole moments, such as the mixed rare gas clusters described below, is that the electric field emitted by the molecules, and therefore the observable signal, is proportional to the transition dipole moment [26] rather than to its square in the case of absorption modulation spectroscopy.

Double resonance capability was implemented into the spectrometer to extend the accessible frequency range, to increase the intensity of higher J transitions, and as an assignment aid. A horn antenna is mounted perpendicularly to the cavity axis about halfway between the centre of the cavity and the pulsed nozzle [27]. Pump radiation

with frequency from the microwave [28] to the millimetre wave region [27] can be introduced. The resulting double resonance spectra can be interpreted in the following way. The molecular sample travels through the pump radiation interaction zone and sees, in effect, a pump radiation pulse that affects population changes in the pump transition energy levels. These population changes are then detected in the subsequent pulsed microwave experiment. The pulsed nature of the experiment makes it possible to apply subtraction schemes and to filter out and detect only the double resonance effects. We make extensive use of the double resonance capability for quantum number assignments and for signal enhancement of higher J transitions, as illustrated in figure 3.

The dipole moment of a complex or cluster is an important quantity that can contain information about both the change in the electronic charge distribution in a molecular monomer upon complex formation and the large amplitude intermolecular motions. Because of this dependence on the internal motions, the complex dipole moment is an additional parameter that can be used to measure the angular anisotropy of the corresponding potential energy surface. We have recently implemented Stark electrodes into our spectrometer for the purpose of dipole moment measurements [29]. The Stark electrodes are 5 mm thick aluminium plates and measure 30×25 cm. The plates are

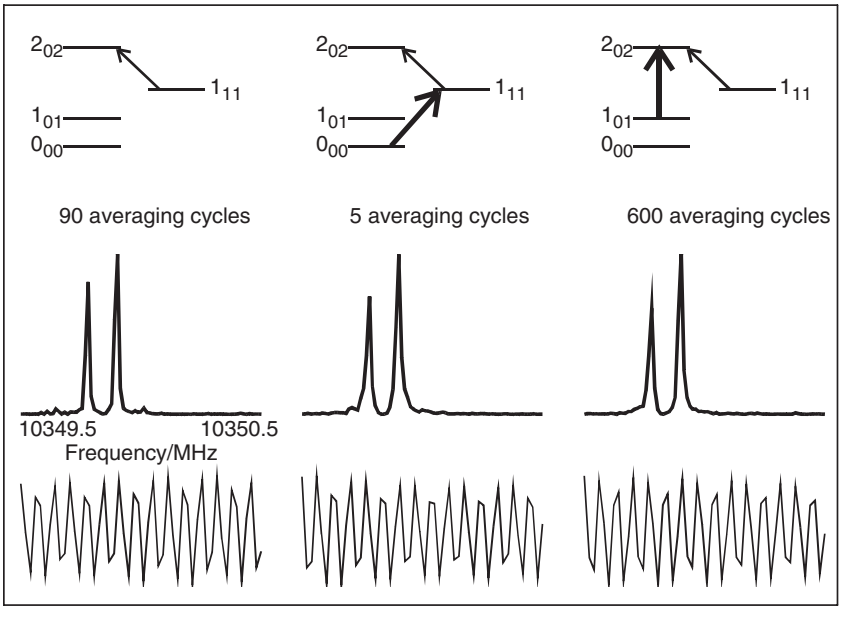

Figure 3. Microwave–Microwave double resonance experiments on the He–OCS complex. The first column shows a single resonance experiment to detect the $J_{K_a,K_c} = 2_{0,2}$–$1_{1,1}$ transition; 90 averaging cycles were needed to achieve a good signal-to-noise ratio. In the next column, microwave pump radiation was applied at a frequency resonant to that of the $J_{K_a,K_c} = 1_{1,1}$–$0_{0,0}$ transition (16841.26 MHz). The pump radiation transfers population from the $0_{0,0}$ into the $1_{1,1}$ level and the signal intensity increases such that only 5 averaging cycles are needed to achieve the same signal-to-noise ratio. If the $2_{0,2}$ level is pumped, however, the population difference between the $1_{1,1}$ and $2_{0,2}$ levels decreases and 600 averaging cycles are now needed. The lowest trace shows the first 40 points of the corresponding time domain signals at sampling interval of 20 ns. With sufficient pump power, a population inversion can be achieved in the signal transition [27]. This would be apparent as a phase inversion in the time domain signal.

mounted at a distance of 30.4 cm apart with the 25 cm long side oriented parallel to the cavity axis. The cavity mirror separation is kept close to 28 cm to minimize electric field inhomogeneities in the cavity. A voltage of up to ±15 kV can be applied, resulting in field strengths of up to 1000 V/cm. The cavity antennas can be oriented parallel or perpendicular to the electric field direction, resulting in selection rules for the quantum number $\Delta M = 0$ and ±1, respectively.

3. Molecular systems

A significant number of ternary and quaternary weakly bound clusters have been studied with the method of Fourier transform microwave spectroscopy. These include (rare gas)$_2$–molecule systems, such as Ar_2–HF [30], Ar_2–HCl [31], Ar_2–HCN [32], Ar_2–H_2O [33], Ar_2–OCS [34], Ne_2–OCS [35], Ar_2–CO_2 [36], Ne_2–N_2O, Ar_2–N_2O [37], Ar_2–HBr [38]; (rare gas)(rare gas)′–molecule trimers, such as NeAr–N_2O [39], NeAr–HCl [40], NeAr–CO_2 [41]; a number of molecule–(molecule′)$_2$ trimers of which we list only a few, e.g. HCl–$(H_2O)_2$ [42], HBr–$(H_2O)_2$ [43], $(HF)_2$–NH_3 [44] $(HCN)_2$–HF, $(HCN)_2$–HCl, $(HCN)_2$–HCF_3, $(HCN)_2$–CO_2 [45], $(HCN)_2$–NH_3, $(HCN)_2$–N_2, $(HCN)_2$–CO, $(HCN)_2$–H_2O [46], HCN–$(CO_2)_2$ [47], HCN–$(CO_2)_3$ [48], $(HCN)_2$–SO_3 [49], $(H_2O)_2$–CO_2 [50], H_2O–$(CO_2)_2$ [51], $(H_2O)_2$–HCOOH, H_2O–$(HCOOH)_2$ [52], $(CO_2)_2$–OCS [53], CO_2–$(OCS)_2$ [54], $(CO_2)_2$–N_2O [55], $(OCS)_2$–HCCH [56], SO_2–$(N_2O)_2$ [57], Ar–$(H_2O)_2$ [58]; and (rare gas)$_3$–molecule tetramers, for example, Ar_3–H_2O, Ar–$(H_2O)_3$ [59], Ar_3–HCN [60], Ar_3–HF [61], Ar_3–H_2S [62]. Below we will outline some of the work that we have been involved in, i.e. the mixed rare gas trimers and tetramers, the ammonia containing $Ne_{2,3}$–NH_3, $Ar_{2,3}$–NH_3, and clusters with helium atoms, i.e. $He_{2,3}$–OCS and $He_{2,3}$–N_2O. For these cases, we will also discuss the rotational spectra of the corresponding binary systems and their interaction potentials, since they form the basis for both the spectroscopic assignments of the larger clusters and possible theoretical extraction of three-body (or higher order) interactions.

3.1. *Mixed rare gas dimers*

The simplest possible complexes and clusters are those that consist only of rare gas atoms. In this case, the interaction potential is greatly simplified because of the reduced number of degrees of freedom. In terms of physical interactions, the dispersion interaction is the only one present in the dimers, and induction interactions come only into play as three- or more-body non-additive contributions. This separation of electrostatic interactions can simplify the analysis of spectra of ternary and higher clusters in terms of the significance of various three-body non-additive terms with different physical origins. As such, pure rare gas clusters provide good test cases for the theoretical treatment of three-body non-additive interactions and provide benchmarks for the evaluation of high quality *ab initio* calculations of intermolecular interactions. The absence of a molecular chromophore, however, presents a problem for pure rotational, microwave spectroscopy. Only in the case of mixed rare gas clusters does a transition dipole moment exist that is entirely provided by the dispersion interactions. The method of Fourier transform microwave spectroscopy is ideal for such

investigations because of its proven high sensitivity for species with small dipole moments. The first spectra of mixed rare gas dimers, i.e. Ne–Xe, Ar–Xe, Kr–Xe [63] and Ne–Kr, Ar–Kr [64] were measured in the Gerry lab in Vancouver, followed by the study of Ne–Ar at NIST and Illinois [65]. The measured signals were surprisingly strong despite the small expected dipole moments on the order of only a few hundredths or thousandths of a Debye. Because of the small dipole moment, a microwave power amplifier was inserted into the excitation arm of the microwave circuit. Typical sample conditions were 1% heavier rare gas in neon as backing gas at pressures of a few atmospheres.

Because of their fundamental importance, the mixed rare gas dimer potentials have been the focus of research efforts for some time. Empirical and semi-empirical potentials for He–Ne, He–Ar, He–Kr, He–Xe [66], Ne–Ar [67], Ne–Kr, Ne–Xe [68], Ar–Kr [69], Ar–Xe, and Kr–Xe [70] dimers exist. More recently, *ab initio* potentials have become available for mixed dimers involving atoms up to Kr, i.e. He–Ne [71], He–Ar, Ne–Ar [71, 72], He–Kr, Ne–Kr, Ar–Kr [73]. Tang and Toennies have recently determined all mixed rare gas potentials from those of the homogenous dimers using a set of combining rules [74].

The strong signals observed allowed the measurement of rotational transitions of several isotopomers in all cases. Values for equilibrium separation and well depth of the corresponding dimer potentials were determined in [63] and [64] by adjusting these parameters in the empirical potentials until best fits with the rotational transition frequencies were achieved. The resulting values are given in table 1, together with those from the empirical and semi-empirical potentials as well as the Tang–Toennies values [74]. There is excellent agreement between the experimental and the Tang–Toennies values (deviations on the order of only 0.1%) thus strongly supporting the validity of the procedure employed in [74]. The empirical potentials underestimate the R_e values by about 0.5%, except for the case of Ne–Ar, where R_o is slightly larger (see table 1). We have analysed the Tang–Toennies mixed rare gas potentials [74] to determine the supported rotational energy levels using LeRoy's program LEVEL [75] and used the corresponding rotational transition frequencies in a fitting procedure similar to that applied for the experimental data. The resulting rotational constants B_o and centrifugal distortion constants D_o are also given in table 1, together with the experimental values. Some fits required the inclusion of the sextic distortion

Table 1. Equilibrium separations, rotational constants, and centrifugal distortion constants of the mixed rare gas dimers from experiment and various potentials.

	R_e/Å			B_o/MHz		D_o/kHz	
	Exp.	Pot.	TT[a]	Exp.	TT[a]	Exp.	TT[a]
Ne–Ar	3.481[b]	3.489[c]	3.477	2914.9[b]	2919.7	231.0[b]	230.3
Ne–Kr	3.648[d]	3.631[e]	3.646	2215.4[d]	2217.8	115.4[d]	120.3
Ne–Xe	3.887[f]	3.861[e]	3.889	1824.8[f]	1822.5	72.79[f]	69.61
Ar–Kr	3.894[d]	3.881[g]	3.889	1198.7[d]	1200.0	11.99[d]	11.49
Ar–Xe	4.092[f]	4.067[h]	4.091	961.3[f]	962.7	6.65[f]	6.56
Kr–Xe	4.201[f]	4.174[h]	4.196	549.7[f]	550.8	1.69[f]	1.84

[a][74], [b][65], [c][67], [d][64], [e][68], [f][63], [g][69], [h][70].

constant H_o to reduce the standard deviation of the fit to the experimental uncertainty. All rotational constants are accurate to about 0.1% (Kr–Xe: 0.2%) or 2.5 MHz (Ne–Ar: 5 MHz) in absolute values. The potentials can truly be considered to be of 'spectroscopic accuracy'. While the high quality of the rotational constants from the potentials is a reflection of the accurate position of the equilibrium distances, the centrifugal distortion constants contain information about the radial anisotropy of the potentials. The experimental values for the quartic centrifugal distortion constants D_o are reproduced to within 5% or 5 kHz in absolute values. This indicates that the slopes of the potentials faithfully reproduce the experiments, at least in the region of the lowest energy levels. We note explicitly that this surprising spectroscopic accuracy of the Tang–Toennies potentials has been achieved without using the microwave spectroscopic data of the mixed dimers for their construction. We analysed the available *ab initio* potentials in a similar way; the deviations for the rotational constants are in the 1% range (Ne–Ar: –0.8% [71, 72], Ne–Kr: +1.21% [73], Ar–Kr: +0.7% [73]). The centrifugal distortion constants show somewhat larger deviations. For Ne–Ar, the calculation with the aug-cc-pV5Z-33221 basis set [71] gives a centrifugal distortion constant that is about 30% too small, indicating that the potential is too steep in the attractive region. The larger basis set in [72] (aug-cc-pV6Z-33211) leads to a centrifugal distortion constant that is 7% too large.

Estimates for the dipole moments of the mixed rare gas dimers were obtained from the values of the optimized $\pi/2$ excitation pulse length and comparison with Stark effect measurements on the Ar–CO_2 complex [76]. The resulting values are on the order of a few thousandths (0.0022 D, Ne–Ar) [65] to about a hundredth (0.014 D, Ar–Xe) [63] of a Debye. The order of magnitude agrees with earlier values deduced from collision induced absorption measurements [77] and dispersion effects corrected Hartree–Fock exchange calculations [78, 79]. We have recently determined *ab initio* values for the dipole moments of the Ne–Ar, Ne–Kr, and Ar–Kr dimers at the CCSD(T) level of theory using aug-cc-pV5Z basis sets for all atoms [80]. An integral-density direct algorithm of the analytic CCSD(T) gradient [81, 82] implemented in the Dalton 2.0 program suite was used [83]. The dipole moment of Ne–Ar was calculated at several separations, from 2.8 to 5.0 Å (see figure 4). At each distance, the counterpoise correction [84, 85] was carried out to account for basis set superposition error. The values were then interpolated using a cubic spline function and averaged over the ground state vibrational wavefunction by numerical integration. The wavefunction was obtained with LeRoy's LEVEL 7.5 program [75] using the Tang–Toennies Ne–Ar potential [74]. The resulting value of the dipole moment is 0.00335 D, with the negative end at the argon atom. This is in good agreement with the value of 0.0022(5) D estimated in [65] from the $\pi/2$ microwave excitation pulse length [63]. The experimental determination of the dipole moment of Ne–Ar was attempted recently by us using Stark effect measurements. At the maximum attainable field strength, however, no shift of the transition frequency of the $J = 1$–0 transition could be detected. The frequency measurements were reproducible to within 200 Hz and a tentative upper value of the dipole moment of 0.005 D was estimated.

Several isotopes of rare gas atoms exist that possess a nuclear spin quantum number $I \geq 1$ and an associated nuclear electric quadrupole moment. The interaction of the

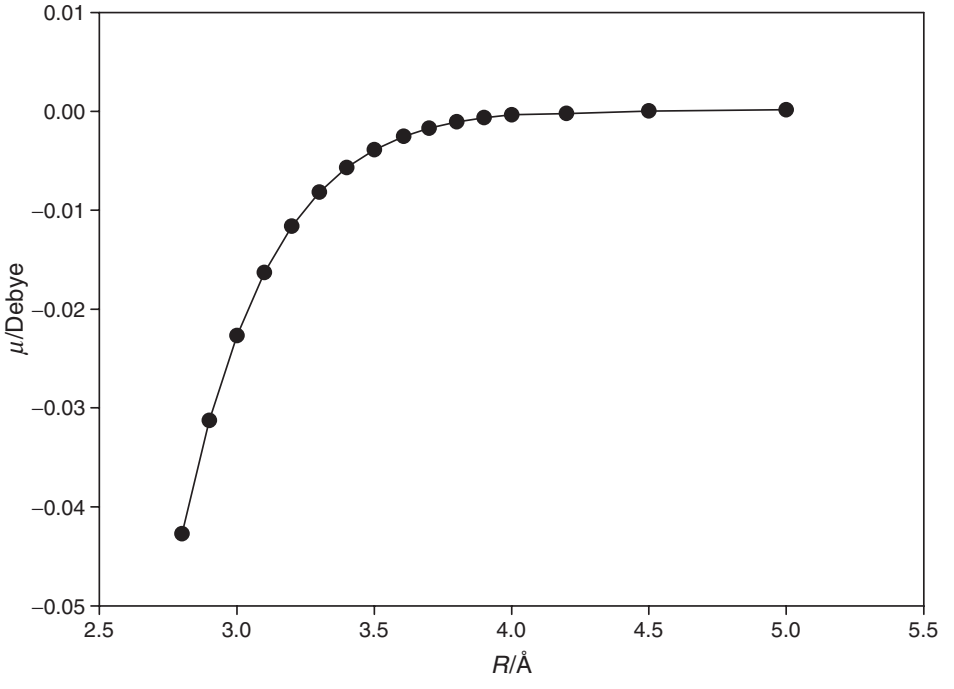

Figure 4. Values of *ab initio* dipole moments of Ne–Ar as a function of bond length. The strong bond length dependence requires averaging over the vibrational wavefunction for comparison with experiment. See the text for details about the calculations. An average value for μ of 0.00335 D was obtained which may be compared to the experimental value of 0.0022(5) D, estimated from the $\pi/2$ excitation pulse length in the microwave experiment [65].

nuclear quadrupole moment with the spherically symmetric electric charge distribution in an isolated rare gas atom does not lead to an energy level splitting. However, the slight distortion of the electron charge cloud in a rare gas dimer leads to a non-zero electric field gradient at the location of the nucleus. The resulting coupling of the nuclear spin with the overall rotational angular momentum of the dimer leads to a splitting of the rotational energy levels and to so-called nuclear quadrupole hyperfine structure in the microwave spectra. Figure 5 shows a spectrum of the ^{20}Ne–^{83}Kr dimer as an example. The resulting nuclear quadrupole coupling constants can be compared with those of rare-gas–molecule dimers. If a molecule is involved, the main contributor to the electric field gradient at the rare gas nucleus is the electric multipole moments of the molecular monomer. Such analyses have been carried out by Legon and co-workers for the cases of ^{83}Kr and ^{131}Xe containing complexes (see figures 4 and 3 of [86]). An extrapolation of the results to the case of zero electric multipole moments of the monomer led to a residual negative nuclear quadrupole coupling constant of -0.44 ± 1.7 MHz for ^{83}Kr and -0.243 ± 1.6 MHz for ^{131}Xe. These values agree qualitatively with the values obtained for the nuclear quadrupole coupling constants in the mixed rare gas dimers. This suggests that dispersion interactions make a non-negligible contribution to the field gradient at the rare gas nucleus

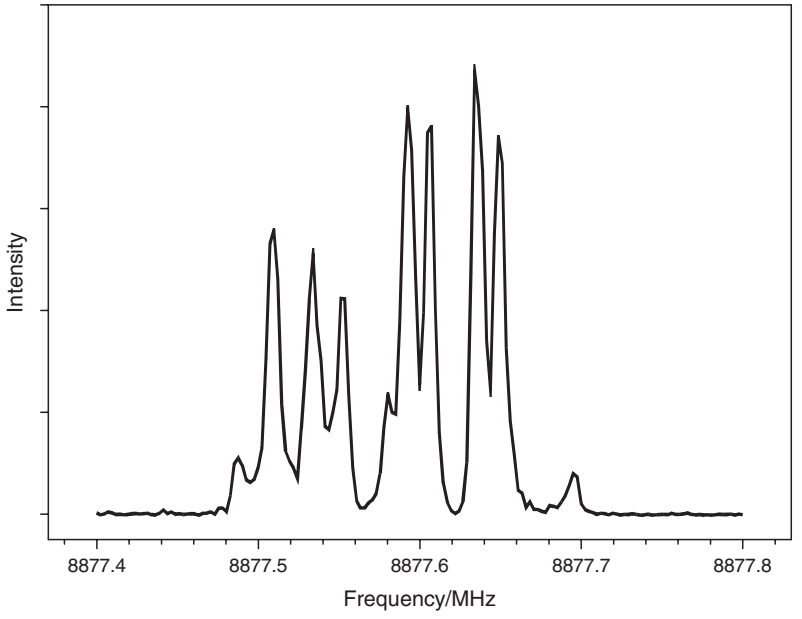

Figure 5. Spectrum of the $J = 2$–1 rotational transition of the ^{20}Ne–^{83}Kr dimer [64]. The ^{83}Kr (nuclear spin quantum number $I = 9/2$) nuclear quadrupole hyperfine structure is partially resolved. The complex was studied in its natural abundance (10.5%) and 500 averaging cycles were used to record the spectrum.

in rare-gas–molecule dimers that is opposite in sign to that produced by the monomer multipole moments.

The nuclear quadrupole coupling constants in the mixed rare gas dimers can be used as sensitive tests of high level *ab initio* calculations, in particular, to determine how well dispersion interactions can be modelled. We have recently calculated molecular electric field gradients at the Ne and Kr nuclei in the Ne–Ar, Ne–Kr, and Ar–Kr dimers [80]. The nuclear quadrupole coupling constant χ for ^{21}Ne is related to the field gradient q along the interatomic axis and to the nuclear quadrupole moment Q of ^{21}Ne by the expression $\chi = 234.964\,73 \cdot Q$ [barn] $\cdot$ q [a.u.]. A procedure similar to that outlined above for the determination of the *ab initio* dipole moment was used. The resulting ^{21}Ne nuclear quadrupole coupling constant of Ne–Ar is shown in figure 6 as a function of the Ne–Ar bond length. Averaging over the ground state wavefunction led to a value of χ of -28.834 kHz, using the Tang–Toennies Ne–Ar potential [74]. This is in excellent agreement with the experimental value of $-30(2)$ kHz [65]. The outstanding correspondence of *ab initio* values for dipole moment and ^{21}Ne nuclear quadrupole coupling constant of the Ne–Ar dimer indicates that highest quality electronic structure calculations are now able to model dispersion interactions faithfully.

There are several interesting outstanding issues with regard to the rotational spectroscopy of rare gas dimers. One such issue is the investigation of helium atom containing dimers. The results of such studies would not only provide further stringent test cases for high quality *ab initio* calculations, but may also contribute valuable

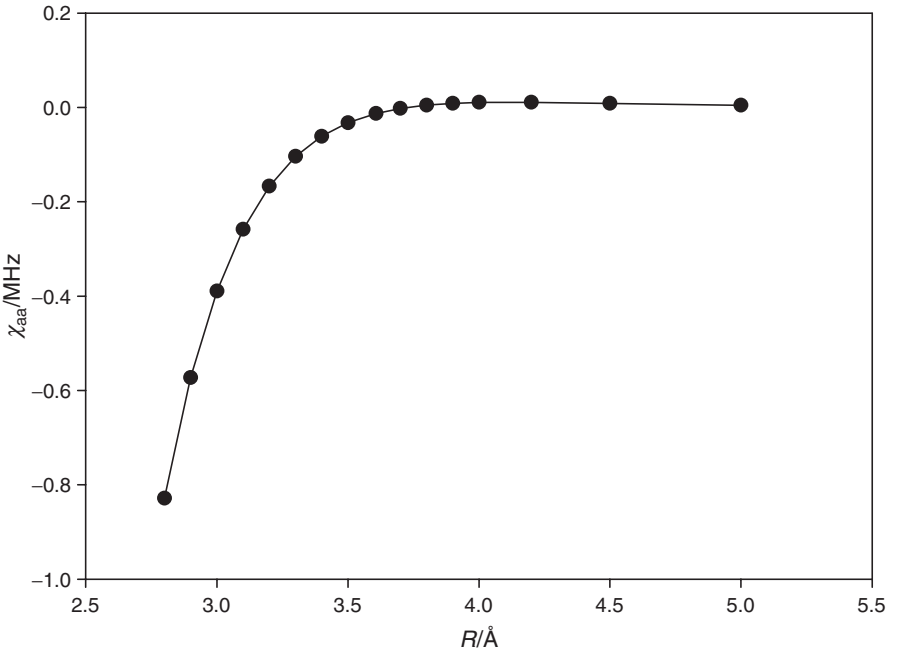

Figure 6. Variation of the *ab initio* ^{21}Ne nuclear quadrupole coupling constant χ of the ^{21}Ne–^{40}Ar dimer with bond length. The strong bond length dependence makes it necessary to average this quantity over the ground state wavefunction for comparison with experiment, as in the case of the dipole moment. An averaged value for χ of −28.834 kHz resulted, compared to the experimental value of −30(2) kHz [65].

information for the improvement of the helium dimer potential. This improvement could possibly be achieved by inverting the combining rule procedure that led to the high-accuracy Tang–Toennies mixed dimer potentials from the homogenous rare gas dimer potentials. The most promising candidate for a spectroscopic investigation is the He–Kr dimer; it is heavy enough to detect several rotational transitions within the frequency range of the spectrometer and has a binding energy that is comparable to that of other weakly bound complexes that have already been investigated. We have searched for the He–Kr spectrum a number of times without success. Possible reasons for the failure are an exceedingly small dipole moment and a larger than anticipated uncertainty in the prediction of the transition frequencies from the available potentials. The other outstanding issue is the investigation of an isotopically substituted homogenous rare gas dimer, for example ^{20}Ne–^{22}Ne. For a homonuclear diatomic molecule, rotational transitions within an electronic state are rigorously forbidden even if breakdown of the Born–Oppenheimer approximation is considered [87]. However, the Born–Oppenheimer breakdown makes rotational transitions allowed for the case of isotopically unsymmetric molecules. Bunker has derived expressions for ro-vibrational transition intensities for the case of HD [87]. Our efforts to detect rotational transitions of ^{20}Ne–^{22}Ne were thus far without success. One possible reason is an extremely small dipole moment that prevents detection of the rotational transitions.

3.2. *Mixed rare gas trimers and tetramers*

The strong signals observed for the mixed rare gas dimers indicated that there was a possibility to also measure rotational microwave transitions of mixed rare gas trimers. Spectra of Ne_2Kr and Ne_2Xe were measured in Vancouver in the Gerry laboratory [88]. Subsequently, the spectra of all possible mixed Ne and Ar containing trimers and tetramers [89] were measured in our laboratory. For these measurements, sample mixtures of 1% Ar in Ne backing gas were used. The application of higher pressures (up to 5 atm) than used for the dimer studies increased the production of trimers and tetramers in the molecular expansion.

It turns out that ternary van der Waals complexes of the type (rare gas)$_2$–molecule/rare gas are often highly asymmetric rotor systems with irregular spectroscopic patterns. This, combined with the large amplitude intermolecular motions of these weakly bound systems, makes the spectroscopic search and assignment procedures extremely challenging. The initial predictions were made by assuming that the trimers are dominated by pairwise additive interactions and the resulting structures have isosceles triangular geometries with C_{2v} symmetry. Similarly, the tetramers form closest packed structures with C_{3v} symmetry for Ne_3–Ar and Ne–Ar_3 and C_{2v} symmetry for Ne_2–Ar_2. Since there are relatively large uncertainties in the bond lengths, especially of the Ne–Ne bond length, the predicted rotational constants were not anticipated to be very accurate. The transitions were found up to one GHz away from the prediction. The final assignments were achieved by using an iterative procedure of spectroscopic fits, predictions, and detection of further transitions, including those of minor isotopomers. The spectroscopic signatures of the Ne_3–Ar and Ne–Ar_3 tetramers are more straightforward since these clusters are symmetric top molecules. However, their lower intensities added to the search difficulties. The spectroscopic assignment of the Ne_2–Ar_2 transitions was the most challenging and could only be achieved by the simultaneous study of several isotopomers. A further complication in the assignment procedure arose in the case of the Ne and Ar containing clusters with the observation of a larger number of transitions with appreciable intensity than originally anticipated. It turns out that there is significant enrichment of heavier isotopomers in the molecular expansion. For example, the intensities of the $J = 1$–0 transitions in the power spectra of $^{20}Ne_2Ar$, $^{22}Ne^{20}NeAr$, and $^{22}Ne_2Ar$ (see figure 7) are in the ratio of 1:1.15:1.38 while the natural abundances are 0.64:16:83.36. The mass increase for the heavier isotopomers results in a lower zero-point energy level and larger dissociation energy. The isotopic enrichment can be explained by the thermal quasi-equilibrium reached as a result of repeated dissociation and re-formation of the rare gas trimers in the low-temperature molecular expansion.

The predicted symmetries of the mixed rare gas trimers and tetramers were confirmed by the observation of the effects of spin statistics in their spectra. The nuclei of ^{20}Ne, ^{22}Ne, and ^{40}Ar, for example, have spin zero and Bose–Einstein statistics apply. As a consequence, half of the energy levels of the isotopomers with C_{2v} symmetry are missing. The resulting energy level diagrams for Ne_2–Ar and Ne–Ar_2 are shown in figures 8 and 9. The difference between the two diagrams reflects that the C_2 axis coincides with the *a*-inertial axis for Ne_2–Ar and with the *b*-axis in Ne–Ar_2. For the species with lower symmetry, such as $^{20}Ne^{22}Ne$–Ar, spin statistical effects do not

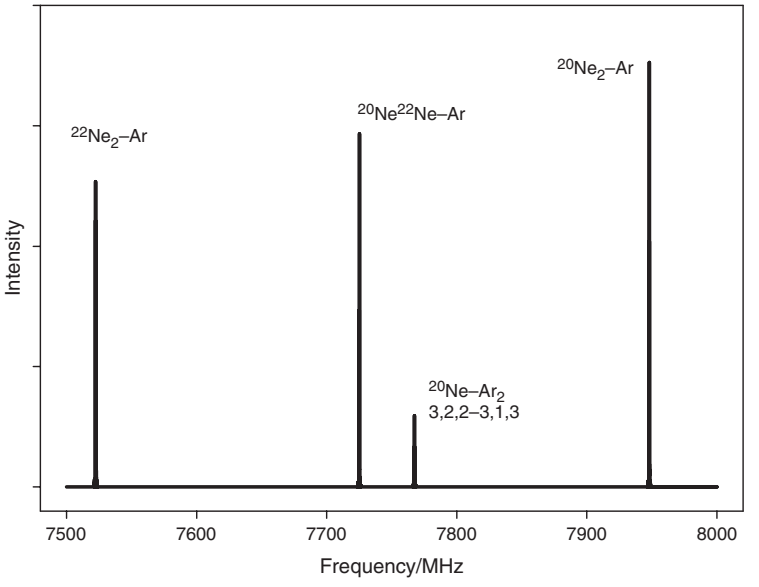

Figure 7. Survey spectrum, using a sample mixture of 1% Ar in Ne at a backing pressure of 5 atm. The $J_{Ka,Kc} = 2_{0,2}$–$1_{0,1}$ transitions of three isotopomers of Ne_2–Ar were detected, together with the $J_{Ka,Kc} = 3_{2,2}$–$3_{1,3}$ transition of Ne–Ar_2. The intensities of the $^{20}Ne^{22}Ne$–Ar and $^{22}Ne_2$–Ar trimers are much higher than expected from the natural abundances. This enhancement is a result of an isotope effect, where the heavier isotopomers are enriched at the low temperatures in the molecular expansion.

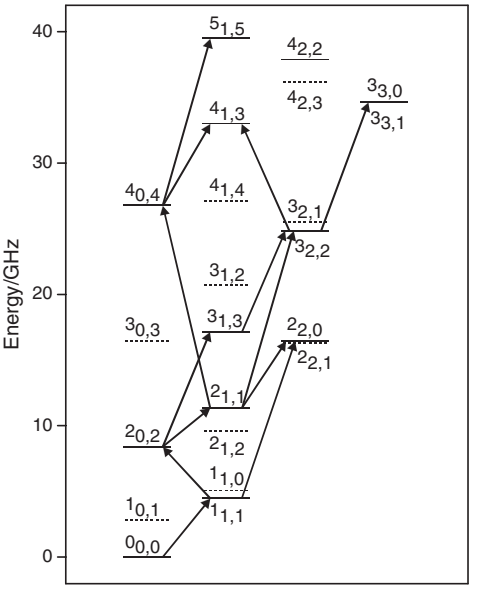

Figure 8. Energy level diagram of the mixed rare gas trimer Ne–Ar_2 [89]. The dashed horizontal lines represent energy levels of the isotopomers with C_{2v} symmetry with zero spin statistical weight. The abundance of the ^{36}Ar isotope is too low to permit the observation of transitions of isotopomers with C_s symmetry.

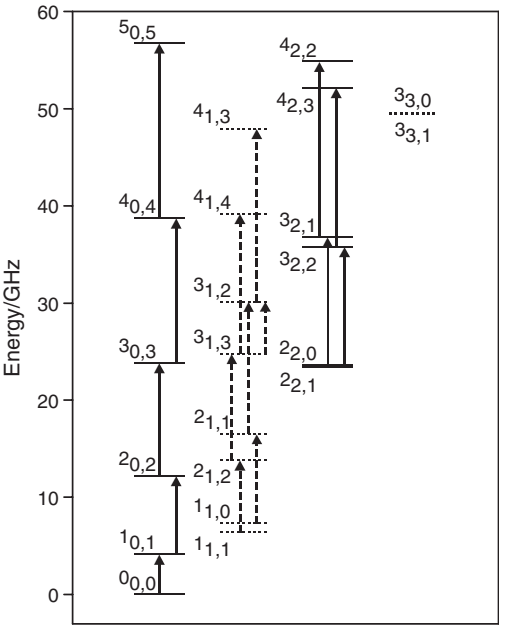

Figure 9. Energy level diagram of the mixed rare gas trimer Ne_2–Ar [89]. The dashed energy levels have spin weight zero for $^{20}Ne_2$–Ar and $^{22}Ne_2$–Ar; however, if the symmetry is broken, as in $^{20}Ne^{22}Ne$–Ar, transitions between these energy levels can also be observed as indicated by the dashed vertical lines.

occur and all energy levels are allowed. In these cases, it was therefore possible to measure additional transitions. Similar spin statistical effects as for the trimers occur also for the rare gas tetramers.

The low dimensionality of the mixed rare gas trimer potentials, compared to molecule containing systems, may suggest that it is possible to extract the effects of three-body non-additive interactions from their spectra. For this purpose, Hutson and co-workers have determined ground state energies and rotational constants for a number of mixed rare-gas trimers [90, 91]. Calculations were done using pairwise additive potentials without and with inclusion of an Axilrod–Teller triple-dipole term [14]. The mixed rare gas dimer potentials were initially adjusted by varying the equilibrium distance until a best agreement with the microwave data was achieved. The resulting rotational constants are given in table 2, together with the experimental values. A first observation is that the theoretical predictions have almost spectroscopic accuracy with deviations to experiment of less than 10 MHz. Such high quality theoretical data are expected to aid the experimental spectroscopic search and assignment procedures greatly. The Ne–Ne pair potential [92] can be assumed to be the least accurate since there were no rotationally resolved spectroscopic data available for its construction. This will mostly affect the accuracy of the A rotational constants in the Ne_2–Ar, Ne_2–Kr, and Ne_2–Xe trimers since the Ne–Ne unit lies perpendicular to the *a*-inertial axis, and to a lesser degree also the C rotational constant. It can be seen from table 2 that inclusion of the Axilrod–Teller term shifts the A constants of Ne_2–Ar and Ne_2–Kr in the right direction, but over-corrects. Ernesti and Hutson have suggested [91] that

Table 2. Rotational constants (in MHz) of the mixed rare gas trimers from pairwise additive calculations, with inclusion of the triple–dipole term [91], and from experiment.

	V_{add}[a]	$V_{\text{add}} + V^{\text{AT}}$	Experiment
$^{20}Ne_2$–^{40}Ar			
A	4742.30 (+8.2)[b]	4730.61 (−3.49)[b]	4734.1 (8)[c]
B	2488.88 (+4.24)	2486.92 (+2.28)	2484.64 (6)
C	1592.57 (−5.31)	1590.09 (−7.79)	1597.88 (6)
$^{20}Ne_2$–^{84}Kr			
A	4730.93 (+3.28)	4718.53 (−9.12)	4727.65 (14)[d]
B	1652.86 (+4.18)	1651.70 (+3.02)	1648.6790 (30)
C	1201.22 (−3.21)	1199.58 (−4.85)	1204.4251 (37)
$^{20}Ne_2$–^{129}Xe			
A	4731.27 (N/A)	4718.90 (N/A)	
B	1261.29 (+0.46)	1260.43 (−0.40)	1260.831 (31)[d]
C	979.99 (+0.01)	978.80 (−1.18)	979.980 (13)
$^{40}Ar_2$–^{20}Ne			
A	3409.49 (+6.72)	3398.72 (−4.05)	3402.7687 (4)[c]
B	1746.20 (+6.48)	1744.44 (+4.72)	1739.7172 (6)
C	1137.30 (+0.00)	1135.14 (−2.16)	1137.2952 (6)

[a]The V_{add} correspond to the 'modified potentials' in [91].
[b]The values in brackets are (theoretical values)–(experimental values).
[c][89]; [d][88].

this overcorrection (in the case of Ne_2–Kr) may be a result of too large an equilibrium separation in the Ne–Ne potential. In all cases, the discrepancy between the experimental and calculated B rotational constant decreases with inclusion of the Axilrod–Teller term. For the C constant, a slight worsening is observed which may again be attributed to inadequacies in the Ne–Ne potential. The high-accuracy new Tang–Toennies potentials for the mixed rare gas dimers [74] may help to more reliably extract three-body forces from the trimer data. The main obstacle, however, is the lack of a Ne–Ne potential with spectroscopic accuracy. The measurement of rotational transitions for the ^{20}Ne–^{22}Ne dimer, as suggested above, would be invaluable for the improvement of the potential.

In the cases of the ^{21}Ne–Ar_2, Ne_2–^{83}Kr, and Ne_2–^{131}Xe trimers it was possible to detect nuclear quadrupole hyperfine structure due to the ^{21}Ne (nuclear spin quantum number $I = 1$), ^{83}Kr ($I = 9/2$), and ^{131}Xe ($I = 5/2$) nuclei, respectively. The resulting nuclear quadrupole coupling constants can be related to those of the corresponding mixed rare gas dimers. For example, the value of the out-of-plane coupling constants χ_{cc} in the trimers is expected to equal $-\chi_{zz}$ of the corresponding dimer under the assumption of pairwise additivity. The uncertainties in the χ_{cc} trimer values are relatively large because only *a*-type transitions were observed. Nevertheless, the experimental values show significant differences to those predicted using pairwise additivity for both Ne_2–^{83}Kr and Ne_2–^{131}Xe. The deviations are 4.9 (74)% for ^{83}Kr and −20.6 (48)% for ^{131}Xe. It appears, from the different signs and magnitudes of the deviations, that the possible three-body effects depend sensitively on the particular rare gas atoms involved and on the structure of the trimers. Similar observations were made in the studies of three-body effects on dipole moments [93, 94].

3.3. *Neon$_{1,2,3}$– and argon$_{1,2,3}$–ammonia clusters*

A step further in complexity is the study of van der Waals complexes consisting of one or more rare gas atoms bound to a molecule. In general, (rare gas)$_N$–molecule systems are viewed as prototypes for probing solvation on the molecular level as rare gas atoms are the simplest solvent with which to study the weak interaction with a particular molecule of interest [95]. Mixed clusters of various sizes are readily formed via molecular beam expansion of gas mixtures. If the appropriate binary potentials are well known (rare-gas–rare-gas, rare-gas–molecule), then the non-additive contributions to the interaction energy of larger clusters can, in principle, be deduced. Due to the nature of the weak interactions involved, the spectra of (rare gas)$_N$–molecule complexes are often complicated by the presence of large amplitude, internal motions of the molecular subunit within the van der Waals complex. These modes typically have frequencies of tens or hundreds of gigahertz [10] and may lead to the observation of one or more tunnelling splittings in the rotational spectrum of the complex. The magnitude of the observed splitting depends sensitively on the potential energy surface that governs the weak interaction while the relative intensity of each individual tunnelling component is dependent on nuclear spin statistical considerations. The latter can be determined by completing a full molecular symmetry group analysis [96].

In recent years, the microwave spectra of a series of van der Waals dimers, trimers and tetramers containing NH_3 with rare gas atoms have been measured in our laboratory. These studies were, in part, inspired by the extensive literature on the Ar–NH_3 complex. For this dimer, the spectra reported in the microwave [97–99] and submillimetre wave [99–102] regions reveal that the NH_3 subunit undergoes large amplitude internal rotation and inversion motions while bound to the Ar atom. This leads to the observation of both internal rotor and inversion tunnelling splittings. The desire to understand and model the complicated dynamics of Ar–NH_3 has fueled several theoretical investigations including the construction and testing of *ab initio* potential energy surfaces [103–110]. These studies provide information about the minimum energy structure, barriers to internal motions and approximate binding energies of the Ar–NH_3 complex. Furthermore, it has been shown for Ar–NH_3 that high quality *ab initio* potential energy surfaces are qualitatively consistent with the empirical potential [111] derived from fitting microwave, submillimetre and far-infrared spectra [112–114]. This suggests that *ab initio* derived potentials capture the essential features of the interaction between Ar and NH_3 and thus provide a means for investigating binary interactions in similar systems for which there is insufficient spectroscopic data to construct an accurate empirical potential. This is an important result because the construction of empirical potentials requires spectroscopic data that is sensitive to a large region of the potential energy surface and Fourier transform microwave spectra alone cannot provide this information.

The presence of multiple internal rotor states and a soft inversion coordinate in NH_3 containing van der Waals complexes provides a unique opportunity to study the interrelationship between the observed spectra and potential energy surface of highly dynamic systems. Of particular interest is the effect of the rare gas binding partner(s) on the internal motions of NH_3 and how the interaction between NH_3 and the rare gas atom(s) changes as a function of the size of the cluster and the polarizability

of the individual rare gas atoms. The complexes studied in our laboratory include Ne–NH_3 [115], Ne_2–NH_3 [116], Ne_3–NH_3 [117], Ar_2–NH_3 [118], Ar_3–NH_3 [119] and Kr–NH_3 [120] as well as the deuterated analogues containing ND_3, ND_2H and NDH_2 for each of these systems and for Ar–NH_3 [121]. These complexes are readily produced in a molecular beam expansion from a gas mixture containing 0.3–0.5% NH_3, 5% Ar or Kr (if applicable) with Ne used as a backing gas to obtain a total sample pressure of 10–12 atm. For the deuterated species, ND_3 gas was used and the ND_2H and NDH_2 isotopomers were subsequently observed due to efficient hydrogen exchange with residual H_2O or NH_3 in the sample system. Isotopomers of the rare gas atoms (^{20}Ne, ^{22}Ne, ^{86}Kr, ^{84}Kr, ^{83}Kr, ^{82}Kr, ^{80}Kr) were measured in their natural abundance.

Due to the low temperatures achieved in the beam ($T < 1$ K), only the lowest energy internal rotor states associated with a unique nuclear spin function are appreciably populated for spectroscopic study in the microwave region. For NH_3 containing complexes, these are the states which correlate with the $j_k = 0_0$ and $j_k = 1_1$ rotational levels of free NH_3 which are associated with *ortho* and *para* nuclear spin functions, respectively. The convention used to label the resulting states of the associated van der Waals cluster is to give the projection (K) of j onto the intermolecular axis in terms of a Greek symbol: Σ ($K = 0$), Π ($K = 1$), etc. followed by j_k. An additional subscript, 'a' or 's', describes the symmetry of the inversion wavefunction as antisymmetric or symmetric, respectively. For each internal rotor state of a (rare gas)$_N$–NH_3 complex associated with an *ortho* nuclear spin function, one of the inversion components has a spin statistical weight of zero and cannot be observed. Substitution of one or more protons (fermions) with deuterons (bosons) changes the spin statistics and the inversion tunnelling components have non-zero weights for all internal rotor states. The observed microwave spectrum consists of a set of rotational transitions for each populated, non-zero spin weighted state of the complex. The transitions of each set are fit to obtain the spectroscopic constants for a particular internal rotor/inversion state of the complex. For the (rare gas)$_N$–NH_3 complexes, the lowest energy state is $\Sigma 0_{0a}$ and its inversion partner is missing due to spin statistical considerations. In Ar–NH_3 and Kr–NH_3, both inversion components of the metastable $\Sigma 1_1$ state have been observed but are heavily perturbed due to Coriolis mixing with nearby Π internal rotor states [99, 120, 121]. These higher energy states have not been observed for the ternary and quaternary clusters.

The approximate minimum energy orientation of NH_3 within the (rare gas)$_N$–NH_3 complexes is shown in figure 10 based on *ab initio* potential energy surfaces computed for the Ne containing systems at the CCSD(T) level [115–117]. Because the NH_3 subunit undergoes large amplitude motions within the clusters, its dipole moment is nearly averaged out and the rotational spectra can essentially be interpreted as if the NH_3 moiety were a sphere. The spectra observed for the dimer complexes: Ne–NH_3, Ar–NH_3 and Kr–NH_3, resemble those of a diatomic molecule with successive transitions spaced by approximately 2B. The bond lengths derived from the rotational constants of the $\Sigma 0_{0a}$ states increase (3.7227 Å, 3.8358 Å, 3.9220 Å) [115, 98, 120] as the magnitude of the van der Waals radii of the rare gas binding partners increase (^{20}Ne, Ar, ^{84}Kr) as expected to accommodate the larger atom. The experimentally determined bond lengths of the dimers are larger than those corresponding to the

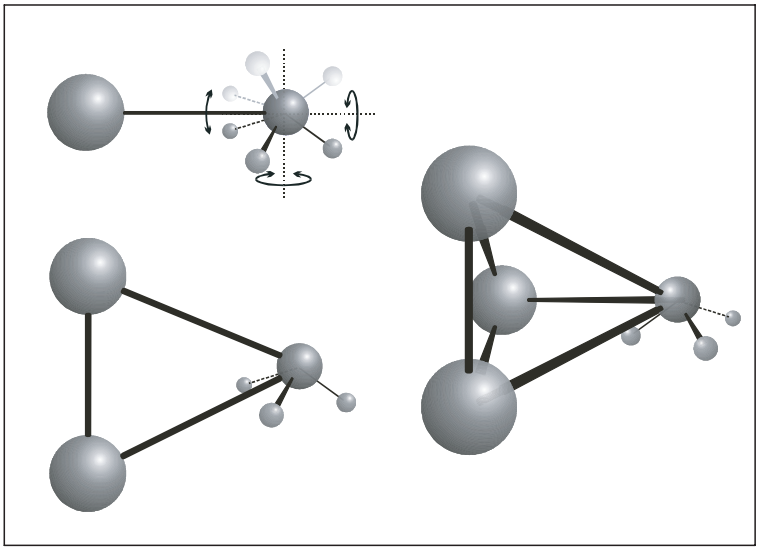

Figure 10. Minimum energy structures of the (rare gas)$_N$–NH_3 clusters. The experimental results and *ab initio* calculations suggest that the NH_3 subunit undergoes large amplitude internal rotation and inversion motions within the complexes and that, on average, the C_3 axis of the NH_3 subunit is oriented perpendicularly to the intermolecular axis joining the centre of mass of NH_3 to the centre of mass of the (rare gas)$_N$ cluster.

global minima of the *ab initio* intermolecular potentials of Ne–NH_3 and Ar–NH_3 at the MP4 level: 3.30 Å and 3.628 Å, respectively [2, 115]. A cut through the potential energy surface of Ne–NH_3 demonstrates that the surface is very flat along the radial coordinate around the minimum energy NH_3 orientation. This suggests that the discrepancy between the experimental and *ab initio* values of R arises from the former being significantly affected by large zero-point vibrations of the dimer.

The ternary species, (rare gas)$_2$–NH_3 are asymmetric tops and their spectra were initially predicted by assuming structures based on the bond lengths from the (rare gas)–NH_3 dimers combined with the Ar–Ar and Ne–Ne separations derived from the spectra of similar clusters such as Ar_2–H_2O [33] and Ne_2–N_2O [37]. The pairwise additive approach gave a good estimate of the rotational constants of Ar_2–NH_3 and $^{20}Ne_2$–NH_3 and the lowest J transitions were found within 25 MHz of the predictions. For the $^{20}Ne_2$–NH_3 and $^{22}Ne_2$–NH_3 complexes, the observed transitions are *a*-type whereas the spectrum of Ar_2–NH_3 is *b*-type due to the different orientation of the principal inertial axis system for the heavier complex. The bilateral symmetry of the cluster is broken in the mixed isotopomer, $^{20}Ne^{22}Ne$–NH_3, and as a result, both *a*- and *b*-type transitions are observed although the latter are extremely weak. As the (rare gas)$_2$–NH_3 complexes are nearly planar (figure 10), the inertial defect, $\Delta_o = I_C - I_B - I_A$, can be calculated from the rotational constants and used as an estimate of the rigidity of the system. If the three hydrogen atoms are assumed to be delocalized over the surface of a sphere with a radius of the N–H bond length, the corrected value of Δ_o is $\sim$6 amu Å^2 for Ar_2–NH_3 and $\sim$8 amu Å^2 for $^{20}Ne_2$–NH_3. For a rigid, planar molecule, Δ_o is zero and for typical chemically bound molecules, such as H_2O, the inertial defects are small ($\Delta_o = 0.0486$ amu Å^2) [122]. The comparably

large values of Δ_o for Ar_2–NH_3 and Ne_2–NH_3 suggest that the complexes are very non-rigid and that the rotational constants are highly averaged over zero-point vibrations of the van der Waals modes within the clusters. If NH_3 is treated as a point mass, the van der Waals bond lengths of the trimers are estimated from moment of inertia equations to be 3.260 Å (Ne–Ne), 3.818 Å (Ar–Ar), 3.695 Å (^{20}Ne–NH_3) and 3.835 Å (Ar–NH_3). The (rare-gas)–NH_3 bond lengths are slightly shorter than those of the binary systems, 3.7227 Å (^{20}Ne–NH_3) and 3.836 Å (Ar–NH_3) and the reductions are of a comparable magnitude to those observed for Ar_2–H_2O [33], Ar_2–Ne and Ne_2–Ar [89]. These subtle but real differences are indicative of the relative importance of three-body non-additive contributions to the interaction energy of a particular cluster. The observation that the bond shortening effect is less pronounced for the Ar containing clusters seems to suggest that the non-additive contributors are less significant than, for example, in Ne containing systems. This statement, however, cannot be verified without a detailed quantum mechanical study of a particular Ar_2–molecule system as the rotational constants from which the van der Waals bond lengths are derived are highly averaged as seen by the large inertial defects in these ternary complexes.

The quaternary clusters, $^{20}Ne_3$–NH_3 and $^{22}Ne_3$–NH_3 are prolate symmetric tops and Ar_3–NH_3 is an oblate symmetric top. The structures were estimated by adopting a pairwise additive approach and the B rotational constants were predicted within 4 MHz of the experimental values. For Ar_3–NH_3, transitions corresponding to both $K=0$ and $K=3$ levels were measured while for the Ne containing systems, only transitions within the $K=0$ stack were observed. As the $K=3$ levels are not metastable, there is likely insufficient population in the higher K levels at the low temperatures achieved in the molecular beam. A complete molecular symmetry group theoretical analysis, including the NH_3 inversion symmetry, confirms that only rotational levels with quantum number $K=3n$ ($n=0,1,2,\ldots$) have non-zero spin statistical weights for the $\Sigma 0_{0a}$ state of the quaternary clusters which belong to the G_{72} group. The $^{20}Ne_2{}^{22}Ne$–NH_3 and $^{20}Ne^{22}Ne_2$–NH_3 isotopomers are asymmetric tops and exhibit *a*- and weak *b*-type and *a*- and weak *c*-type transitions, respectively. The molecular symmetry group is different for these systems (G_{24}) and all rotational energy levels are present for the $\Sigma 0_{0a}$ state. Assuming a spherical geometry for NH_3, a moment of inertia equation based on the B rotational constant can be used to estimate the van der Waals bond lengths of the symmetric top clusters $^{20}Ne_3$–NH_3 and Ar_3–NH_3, as shown for Ar_3–H_2O [59]. The Ne–Ne (3.260 Å) and Ar–Ar (3.818 Å) bonds are longer than those extracted for the ternary (rare gas)$_2$–NH_3 clusters by 0.128 Å and 0.048 Å, respectively. Conversely, the (rare gas)–NH_3 bonds are shorter by 0.014 Å and 0.019 Å for Ne–NH_3 (3.681 Å) and Ar–NH_3 (3.814 Å), respectively, when compared to the ternary complexes. Similar trends were observed in the van der Waals bond lengths of Ar_3–H_2O [59], Ar_3Ne and Ne_3Ar [89] and suggest that non-additive contributions to the interaction energies of quaternary clusters are not negligible. Furthermore, these results clearly demonstrate that the magnitude of non-additive effects is influenced by the properties of the rare gas binding partners and thus the construction of accurate models of weak intermolecular interactions will critically depend on the availability of spectroscopic information for molecules solvated by different rare gas atoms.

Table 3. ^{14}N Nuclear quadrupole coupling constants (in MHz) of (rare gas)$_{1,2,3}$–ammonia clusters.

		–ND_3	–ND_2H	–NDH_2	–NH_3	Reference
χ_{aa}	^{20}Ne–	0.5230	0.4401	0.3501	0.2700	[115]
	Ar–	0.6846	0.5698	0.4617	0.350	[99]
	^{84}Kr–	0.5182	0.4252	0.3489	0.2485	[120]
χ_{aa}	$^{20}Ne_2$–	0.636	0.528	0.439	0.335	[116]
χ_{bb}	Ar_2–	1.2490	1.0223	0.8191	0.6221	[118]
χ_{aa}	$^{20}Ne_3$–	0.6943	0.6429	0.5007	0.3939	[117]
χ_{cc}	Ar_3–	0.3221	0.2914	0.2180	0.1458	[119]

The presence of ^{14}N nuclear quadrupole hyperfine structures helped with the assignment of the rotational transitions of the various (rare gas)$_N$–NH_3 species. Because the NH_3 subunit undergoes large amplitude motions in each of these systems, the ^{14}N nuclear quadrupole constants (χ_{aa}, χ_{bb} and/or χ_{cc}) determined from fitting the spectra are intrinsically dependent on these internal dynamics. Assuming that the nuclear quadrupole coupling constant of free NH_3 ($\chi_o = -4.0898$ MHz) [123] is unaffected by the weak interaction, the ^{14}N quadrupole coupling constant of the complex corresponding to the axis linking the centre of mass of NH_3 with the centre of mass of the (rare gas)$_N$ cluster is given by the equation: $\chi_{aa} = \chi_o\langle 3\cos^2\theta - 1\rangle/2$; where χ_{bb} or χ_{cc} replace χ_{aa} as necessary and θ is the angle between the C_3 axis of NH_3 and the *a*, *b* or *c* principal inertial axis of the cluster. In the limit of free internal rotation of NH_3 within each complex, the Legendre factor, $P_2(\cos\theta) = \langle 3\cos^2\theta - 1\rangle/2$, will be zero and the corresponding nuclear quadrupole coupling constant will, therefore, also be zero. Thus, the magnitude of the ^{14}N quadrupole coupling constant obtained from fitting the hyperfine patterns provides information about the relative ease of the internal rotation of NH_3 within the cluster. Table 3 gives the χ values determined for the various (rare gas)$_N$–NH_3 systems. Upon successive deuterium substitution, the χ values increase for each cluster due to the heavier tunnelling mass and lower zero-point energies of the deuterated isotopomers. For the $Ne_{1,2,3}$–NH_3 family, the χ_{aa} values decrease as successive Ne atoms are added to the system, suggesting that the barriers to internal rotation in the θ coordinate increase with cluster size. This is supported by the *ab initio* potential energy surfaces of the three Ne containing systems. The barriers for rotation through $\theta = 180^\circ$ are similar for all three complexes ($\sim$20 cm^{-1}); however, the barriers through $\theta = 0^\circ$: 32.5 cm^{-1} (Ne–NH_3), 38.6 cm^{-1} (Ne_2–NH_3) and 45.0 cm^{-1} (Ne_3–NH_3), increase as a function of cluster size as shown in figure 11. The plots of the θ dependence of the clusters also reveal that the potential wells become broader with the addition of Ne atoms. This lowers the tunnelling probability for internal rotation in the θ coordinate. By comparison, it is somewhat surprising that the χ_{cc} value for Ar_3–NH_3 is considerably smaller than the χ_{aa} value of Ar–NH_3 and χ_{bb} of Ar_2–NH_3. This implies that the barrier to internal rotation is smallest in the quaternary cluster and that the NH_3 molecule experiences a more isotropic environment when bound to three Ar atoms instead of one or two. As more rare gas atoms are added and the bulk phase limit is approached, the internal rotation within the cluster should become less and less hindered. This is supported by experiments involving solid rare gas (Ne, Ar, Kr, Xe) matrices in which NH_3 undergoes nearly free internal rotation [124].

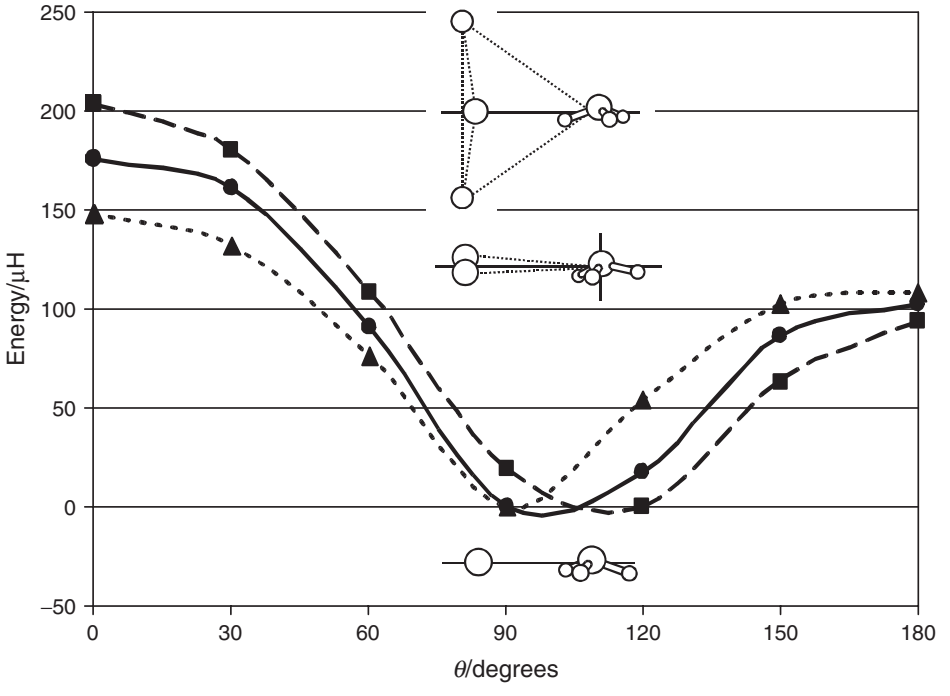

Figure 11. Minimum energy [CCSD(T)] paths of the Ne–NH_3 dimer (- -■- -), the Ne_2–NH_3 (—●—) trimer, and the Ne_3–NH_3 tetramer (– –▲– –) as a function of the θ coordinate for $\angle HNH = 106.67^\circ$ [117]. The dimer and trimer minimum energy paths correspond to the $\phi = 60^\circ$ orientation while the tetramer path corresponds to $\phi = 0^\circ$. The global minimum of each curve was set to 0.0 μH and the other energies along the minimum energy paths were adjusted accordingly.

The seemingly contradictory results for the Ar and Ne containing quaternary systems indicate that the internal motions of NH_3 are highly influenced by the properties of the individual rare gas atoms at this level of solvation. With the addition of more Ne atoms to the cluster, it is thus expected that the interaction will become more isotropic in the θ coordinate and the ^{14}N quadrupole coupling constant will decrease accordingly.

In addition to large amplitude motions in the angular coordinates of the complexes, the NH_3 subunit can undergo inversion while bound to rare gas atoms. As stated earlier, the investigation of deuterated isotopomers provides the opportunity to observe both inversion components of the ground internal rotor state, $\Sigma 0_0$, of the (rare gas)$_N$–NH_3 complexes. This is a direct consequence of the different symmetries of the nuclear spin functions for fermions (protons) and bosons (deuterons). The observed microwave spectra for the deuterated species contain two sets of rotational transitions, one assigned to each inversion tunnelling component, $\Sigma 0_{0s}$ and $\Sigma 0_{0a}$. The energy separation of the inversion states cannot be measured directly as they are associated with different nuclear spin functions but the magnitude of the observed tunnelling splitting provides an indication of the relative energies of the $\Sigma 0_{0s}$ and $\Sigma 0_{0a}$ components since in general, states with similar energies are characterized by similar rotational constants. The differences in the rotational constants of the two inversion

Table 4. Comparison of inversion tunnelling splittings (in kHz) for the (rare gas)–NH_3, (rare gas)$_2$–NH_3, and (rare gas)$_3$–NH_3 complexes.

	–ND_3	–ND_2H	–NDH_2	Reference
$^{20}Ne_3$[a]	−9.4	122.2	473.4	[117]
$^{20}Ne_2$[b]	19.9	298.1	906.2	[116]
Ne[a]	55	407.6	1082.2	[115]
Ar_3[a]	−36	21.4	200.4	[119]
Ar_2[c]	−165.1	36.1	712	[118]
Ar[a]	−63	271.6	1101	[99]
Kr[a]	−85.6	208.4	1038.4	[120]

[a] $2(B_{antisymmetric} - B_{symmetric})$.
[b] $(B+C)_{antisymmetric} - (B+C)_{symmetric}$.
[c] $(A+C)_{antisymmetric} - (A+C)_{symmetric}$.

components of the (rare gas)$_N$–ND_3, –ND_2H and –NDH_2 complexes are given in table 4 and sample spectra for the deuterated isotopomers of Ar_3–NH_3 are shown in figure 12. In all clusters, the observed inversion tunnelling splitting increases with successive hydrogen substitution. This result is consistent with the known energy differences of the inversion levels in free ND_3 (1.6 GHz) [125], ND_2H (5 GHz) and NDH_2 (12 GHz) [126] and with the inversion tunnelling splittings measured by Jacox *et al.* in the infrared region for these species embedded in solid Ne and Ar matrices [127]. Upon comparison of the inversion tunnelling splittings as a function of the number of rare gas atoms, it can be seen that for the Ne containing clusters, the tunnelling splitting decreases with increasing cluster size. This suggests that the inversion is being hindered by the additions of rare gas binding partners. For Ar, the same trend is observed for the binary and ternary systems, but the tunnelling splitting then increases for the Ar_3 containing species suggesting that the inversion is less restricted in the larger cluster. Such comparisons are interesting but should be made with caution as the observed tunnelling splittings provide only secondary indicators of the inversion and are not direct measurements of the inversion mode. The observation of both tunnelling components of the deuterated (rare gas)$_N$–NH_3 clusters is an important result on its own as it confirms that the inversion motion is not quenched by the weak interaction with rare gas atoms. Furthermore, it provides information about the relative orientation of the NH_3 moiety within these complexes as the inversion motion will be quenched unless it occurs along a symmetric coordinate [99]. This suggests that the NH_3 molecule is, on average, oriented with its C_3 axis perpendicular to the intermolecular axis connecting it to the (rare gas)$_n$ cluster as shown in figure 10. The *ab initio* potential energy surfaces of the $Ne_{1,2,3}$–NH_3 species support this observation as they reveal that the interaction energy is insensitive to the ∠HNH angle of NH_3 for orientations around the global minimum. This is shown in figure 13 for the ternary Ne_2–NH_3 complex. At orientations far from the minimum, such as $\theta = 180^\circ$, the internal geometry of NH_3 has a larger effect on the interaction energy. This particular orientation corresponds to a Π internal rotor state and for Ar–NH_3, the inversion was found to be nearly quenched in such a state [99].

The investigations of the (rare gas)$_N$–NH_3 systems described above are a successful demonstration of the power of combining high resolution microwave spectroscopy with

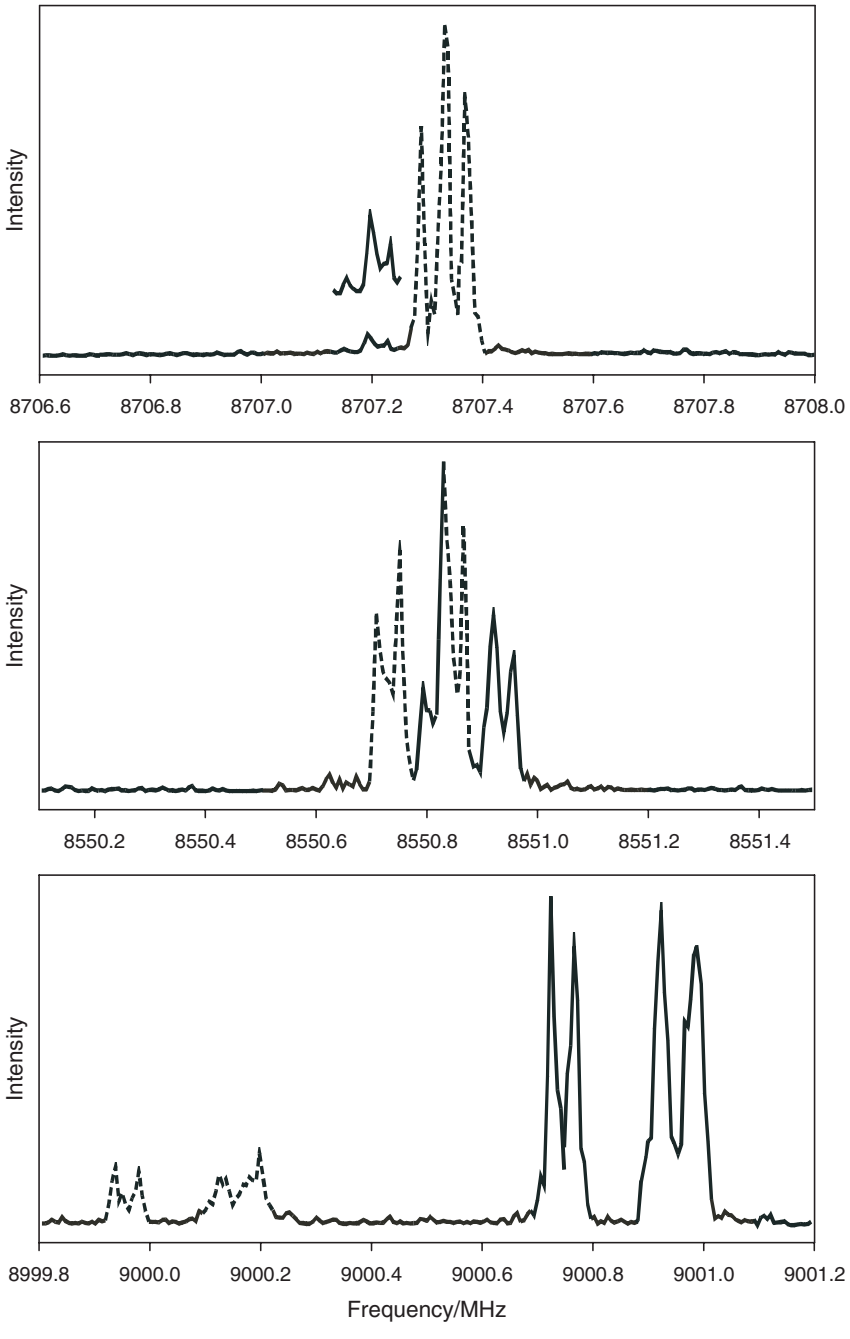

Figure 12. Sample spectra showing the inversion tunnelling splittings of the $J = 3$–4 transitions of the deuterated isotopomers of Ar_3–NH_3. The relative intensities of the tunnelling components are governed by nuclear spin statistics and confirm the assignments. The transitions drawn in dashed (solid) lines correspond to the symmetric (antisymmetric) tunnelling components. The inset in the upper trace shows the intensity of the antisymmetric tunnelling component scaled by a factor of 5.

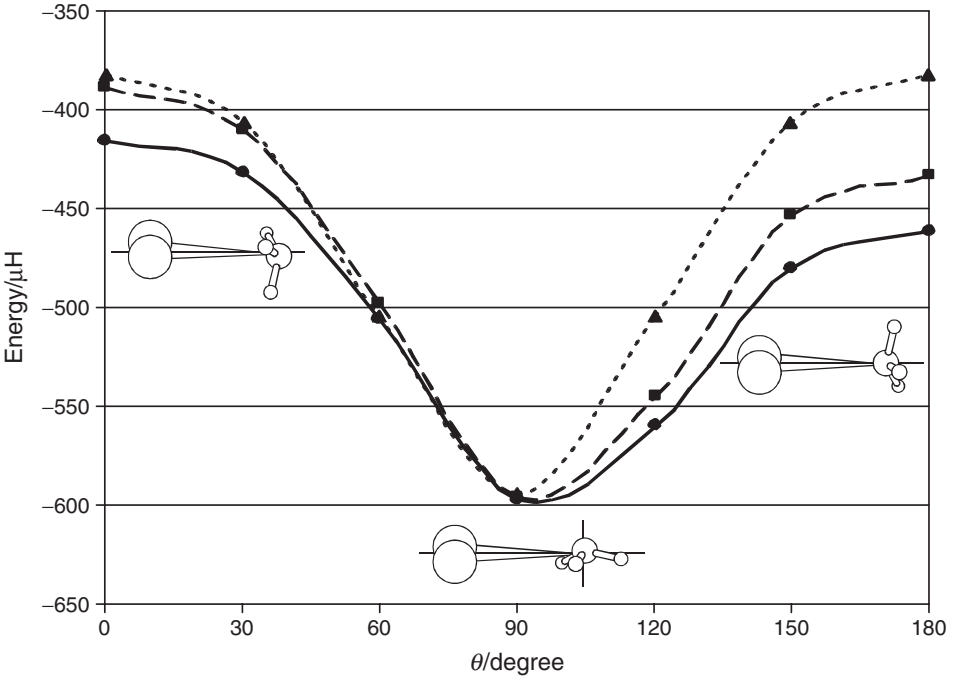

Figure 13. Minimum energy [CCSD(T)] paths of Ne_2–NH_3 as a function of the θ coordinate for $\phi = 60^\circ$, $\beta = 90^\circ$ [116]. Each curve represents a different umbrella angle of NH_2: $\angle HNH = 106.67^\circ$ (—●—), $\angle HNH = 113.34^\circ$ (– –■– –), and $\angle HNH = 120.00^\circ$ (- - ▲- -).

ab initio calculations to monitor the changes in the structural and dynamical properties of these complexes as a function of the number and size of the rare gas binding partners. Since the bulk phase behaviour of these systems can be deduced from spectroscopic studies of NH_3 (or another molecule of interest) in cryogenic rare gas matrices, detailed studies of van der Waals molecules provide important information about intermolecular interactions in the intermediate regime where many-body effects can be isolated. Due to the inverse dependence of the rotational constants on the reduced mass of the cluster, the lowest J transitions of heavier clusters, which are typically the strongest as a result of the Boltzmann populations of the levels involved, lie outside the operational range of microwave spectrometers. This places a limit on the size of the clusters that can be investigated with Ne or Ar as the solvating atoms. Helium containing van der Waals complexes are, therefore, an attractive alternative as the bulk phase behaviour of the system can be better approached.

3.4. *Helium$_{1,2,3}$–molecule complexes*

It is the particularly low binding energies of only a few tens of wavenumbers that make He atom containing complexes and clusters so interesting for spectroscopy and theory. They provide, for example, the most stringent test cases for *ab initio* calculations because of the need to capture the dispersion interaction of the not very polarizable

helium atom accurately. From a purely spectroscopic point of view, it is the extremely large amplitude zero-point vibrations that provide both interest and challenge. The zero-point energy level of He–molecule systems can lie at more than half the well depth because of the weak binding and the low mass of the helium atom. The lowest energy levels are therefore significantly delocalized over both radial and angular coordinates and even pure rotational spectra sample a considerable portion of the potential energy surface.

Another impetus for the study of He–molecule systems is given by the development and applications of the method of helium nanodroplet isolation spectroscopy [128–132]. In this method, helium nanodroplets that consist of 10^3–10^5 helium atoms are generated and assume a temperature of 0.38 K. These droplets can then be doped with molecular or atomic impurities. Closed shell molecular dopants reside in the centre of the droplet and can be interrogated using spectroscopic methods. The resulting spectra, for example infrared spectra, show sharp, rotationally resolved lines and are essentially gas phase-like. The free rotation of the dopant molecules has been interpreted in terms of microscopic superfluidity of the helium droplets. Analysis of the droplet spectra results in a decreased apparent B rotational constant compared to the gas phase value and a shift of the vibrational band origin. Both renormalization of the B constant and vibrational band shift have been investigated in the intermediate cluster size regime as a function of number of helium atoms experimentally for $He_{3–8}$–OCS [28, 133, 134], $He_{3–12}$–N_2O [135], He_N–CO_2 [136, 137], He_N–CO [138–140], and theoretically [141], for example, for He_N–OCS [142–145], He_N–N_2O [146, 147], He_N–CO_2 [137].

The theoretical modelling of He_N–molecule clusters and extraction of accurate spectroscopic parameters for comparison with experimental results require interaction potential energy surfaces of the highest quality. In particular, the surface needs to be accurate not only near the potential minimum, but also at higher energies. For He_N–OCS, for example, it was observed that the first five helium atoms form a doughnut ring around the OCS molecule near the location of the potential minimum. Helium atoms six and seven spill out then into a secondary minimum near the oxygen end and helium atom eight goes into the region of a saddle point at the sulfur end [28, 133, 134]. Observable structure in the trend of the B rotational constant with N in larger clusters [135] indicates that even longer range interactions need to be reproduced very accurately to account for the experimental results.

High-resolution rotational spectra of He–molecule complexes are an exquisite probe of their interaction potentials. In particular, the spectra are sensitive not only to the region of the global minimum, but also to higher energy features mainly because of the high zero-point energy and the resulting large amplitude internal motions. The Klemperer group has measured some of the first rotational spectra of He–molecule complexes, namely He–HCN [148], He–ClF [149], and He–OCS [150] using the method of molecular beam electric resonance spectroscopy. Several further He–molecule complexes have been studied in the infrared (He–CO_2 [151], He–CO [152], He–OCS [153, 154], and He–N_2O] [154], microwave [He–CO [152], He–CO_2 [155], He–N_2O [7], He–HCCCN [156]) and millimetre wave regions (He–HCN) [8]. The spectroscopic experiments on helium droplets doped with OCS [157, 158] have sparked particular interest in the He–OCS potential energy surface. Several high quality He–OCS *ab initio* surfaces have been constructed [147, 150, 159] and adjusted to reproduce the

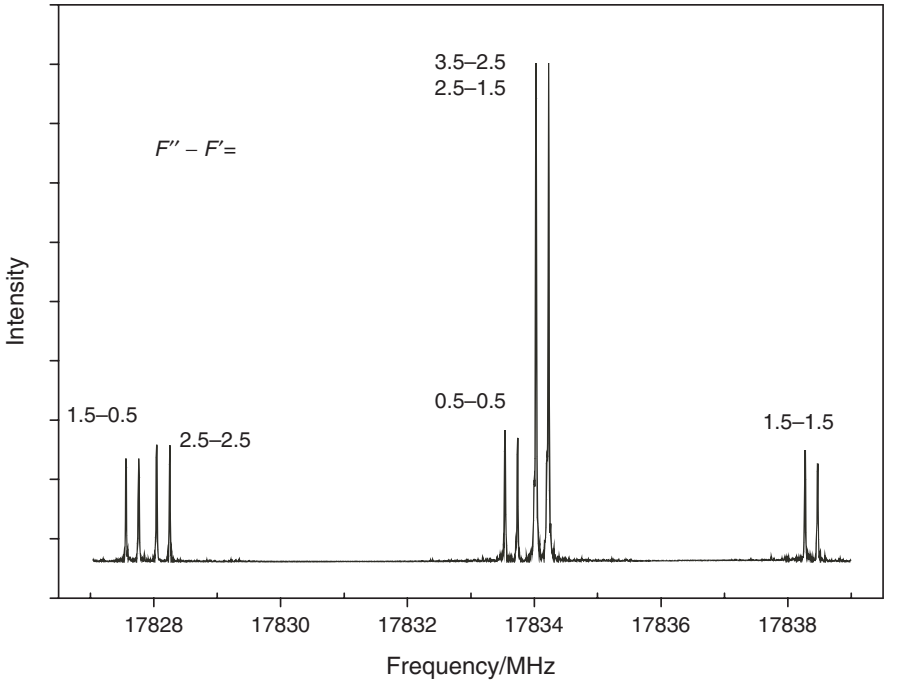

Figure 14. $J_{K_a,K_c}=2_{0,2}$–$1_{0,1}$ transition of He–OC^{33}S. The ^{33}S nuclear quadrupole hyperfine structure is well resolved. The spectrum of He–OC^{33}S was measured in its natural abundance of 0.76%.

rotational transition frequencies. Additional information from the experimental spectra other than the rotational transition frequencies can be used to gauge and to improve potential energy surfaces. For example, isotopic data, nuclear quadrupole hyperfine coupling constants, and dipole moments can be obtained from experiment and compared to the corresponding data extracted from the potential energy surface. We have recently extended the spectroscopic work on He–OCS by measuring transitions of several minor isotopomers, including He–O^{13}CS, He–OC^{34}S, and He–OC^{33}S [160]. Figure 14 shows the well resolved ^{33}S (nuclear spin quantum number $I=3/2$) nuclear quadrupole hyperfine structure of the $J_{K_a,K_c}=2_{0,2}$–$1_{0,1}$ transition of He–OC^{33}S. The nuclear quadrupole coupling constants of the complex are determined by the corresponding monomer constant, assuming that the electronic structure of the molecule does not change upon complex formation with a helium atom, averaged over the appropriate wavefunction of the complex. We found that the ^{33}S nuclear quadrupole coupling constant is K_a dependent and it was necessary to carry out three separate fits for transitions in the $K_a=0$, $+1$, and -1 energy level stacks. Similar behaviour was previously found, for example, in the cases of Ne– [161], Ar– [162, 163], Kr– [164], Xe–N_2 [165]. Hutson and co-workers have explicitly considered the complications due to the large amplitude angular motions for the determination of nuclear quadrupole coupling constants of weakly bound complexes [166–168]. Nuclear quadrupole coupling constants have been used, for example, to improve the potential energy surfaces of He–HCN [168, 169] and He–N_2O [170]. We are currently in the process

of implementing the additional experimental isotopic and nuclear quadrupole data for improvement of the He–OCS potential energy surface [171]. We have very recently also succeeded in measuring the dipole moment of He–OCS using Stark measurements with a static electric field implemented into our microwave Fourier transform spectrometer. Dipole moment components of $\mu_a = 0.6604(16)$ D and $\mu_b = 0.263(13)$ D were obtained [172]. The total dipole moment of the complex $\mu_{tot} = 0.711(13)$ D agrees with the monomer value of 0.715196 D [173], supporting the assumptions of negligible perturbation of the electric properties of the molecular monomer upon complex formation with a helium atom. This is further confirmed by considering the dipole moments of other rare-gas–OCS complexes. The dipole moment decreases in the series Ne–OCS [0.707(13) D], Ar–OCS [0.700(3) D], Kr–OCS [0.696(4) D] [174], which is indicative of increased perturbation with a heavier rare gas binding partner.

The strong signals we observed for He–OCS and its isotopomers, combined with our experience in measuring a number of other (rare gas)$_2$–molecule trimers, such as Ne_2–N_2O, Ar_2–N_2O [37], NeAr–N_2O [39], NeAr–HCl [40], NeAr–CO_2 [41], Ne_2–OCS [35], encouraged us to search for the spectrum of He_2–OCS. There existed no previous rotational or ro-vibrational studies on He_N–molecule systems with $N \geq 2$, mainly because of the anticipated difficulties in producing these clusters in sufficient quantity, even in a molecular beam environment, and also because of their complex spectral pattern that are a result of the very large amplitude intermolecular motions. A traditional method for the prediction of rotational constants for van der Waals complexes is to assume a rigid structure with effective separations and bond angles. However, in the case of a very weakly bound and fluxional system like He_2–OCS, the concept of a ground-state structure is not valid in the sense that a rigid structure that can reproduce the experimental rotational constants does not exist. Initially, we assumed a planar, asymmetric top structure for He_2–OCS, effectively neglecting the He–He interaction. Not unexpectedly, we encountered significant problems in finding and assigning rotational transitions of the He_2–OCS complex. In our initial experiments, one line, namely the $J_{K_a,K_c} = 1_{0,1}$–$0_{0,0}$ transition, was found. The assignment to the quantum numbers and to the molecular carrier, i.e. He_2–OCS, was confirmed by finding the corresponding lines of seven minor isotopomers [175]. Further support came from the nuclear quadrupole hyperfine structures of the $J_{K_a,K_c} = 1_{0,1}$–$0_{0,0}$ rotational transitions of He_2–$OC^{33}S$ and He_2–$^{17}O^{13}CS$ (^{17}O nuclear spin quantum number $I = 5/2$) shown in figures 15 and 16. It was noticed that the line intensities were strongly sample pressure-dependent and dropped significantly below 7 atmospheres. Transition intensities of the He–OCS lines showed similar behaviour, but the effect was much less pronounced. This strong pressure dependence indicates that the transitions are indeed due to a cluster that contains more than one helium atom.

Despite tremendous search efforts, we were initially unable to find the $J_{K_a,K_c} = 2_{0,2}$–$1_{0,1}$ transition of any of the isotopomers. One problem was that scanning of large frequency ranges can be tedious with the method of Fourier transform microwave spectroscopy. (See, however, the recent work by Pate and co-workers [176].) At this point, the advantage of mid-infrared fast-scanning spectroscopy, namely the ability to scan relative large frequency ranges with ease, brought the assignment procedure back on track. The extremely high resolution capability of Fourier transform microwave spectroscopy then complements this advantage of infrared spectroscopy and

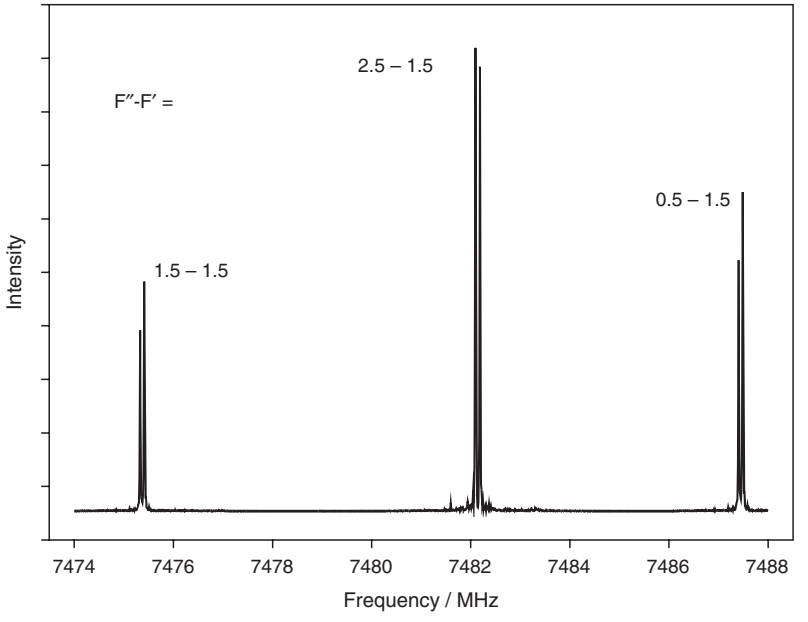

Figure 15. Spectrum showing the ^{33}S nuclear quadrupole hyperfine structure of the $J_{K_a,K_c} = 1_{0,1}$–$0_{0,0}$ transition of He_2–$OC^{33}S$ [175]. The observed hyperfine structure confirms that the complex contains the OCS unit, and was essential for the quantum number assignment.

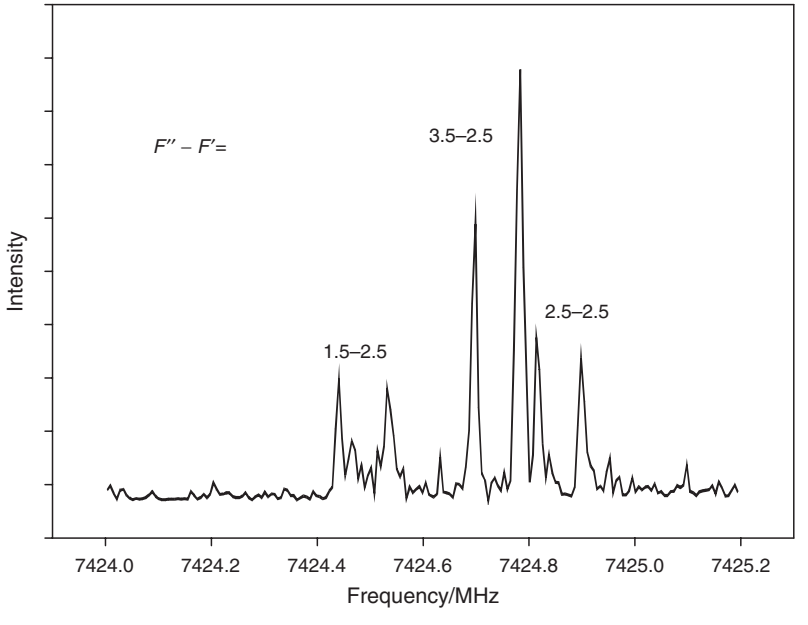

Figure 16. ^{17}O nuclear quadrupole hyperfine structure of the $J_{K_a,K_c} = 1_{0,1}$–$0_{0,0}$ transition of He_2–$^{17}O^{13}CS$ [175]. An enriched sample of $O^{13}CS$ (99% ^{13}C, ~12% ^{18}O) was used. We found that ^{17}O was enriched in this sample to a similar relative extent as ^{18}O.

has been utilized to confirm assignments or to select between different assignment possibilities. The new infrared measurements by Tang and McKellar [133, 134] produced microwave predictions, and we found additional rotational transitions, namely $J_{K_a,K_c} = 2_{0,2}–1_{0,1}$ and $3_{0,3}–2_{0,2}$, for several isotopomers [28]. The final analysis of microwave and infrared data for He_2–OCS in terms of an asymmetric rotor model led to rotational constants that are consistent with the shape of a distorted tetrahedron, similar to the case of Ne_2–OCS [35]. The following structural parameters were derived: the distance R between the centre of mass of OCS to He = 3.8 Å; the angle between the OCS axis and $R = 66°$; the dihedral angle = 188° [134].

There is the possibility of a tunnelling motion of the helium atoms through the planar geometry of the cluster. Spin statistics due to the two equivalent spin zero helium nuclei dictate that the ground state has only even K_a values while the first excited tunnelling state has only odd K_a values. Some tentative candidates for transitions with higher K_a values have been observed in the infrared work, but no additional transitions were found in the microwave range. A plausible reason is the low population of higher energy levels that prevent detection of these transitions. This is in part a result of the higher sample pressures needed for observation of He_2–OCS transitions which, in turn, leads to a significant decrease of the effective rotational temperature in the molecular expansion.

Tang and McKellar's infrared spectra of $He_{1,2}$–OCS contained additional lines that showed even stronger sample pressure dependence than those of He_2–OCS. They were attributed to He_3–OCS, and the assignment was confirmed by finding the corresponding microwave transitions close to the predicted frequencies. The signal strengths were still sufficient to record spectra of several isotopomers; an example spectrum of He_3–$OC^{33}S$ is shown in figure 17. The ^{33}S nuclear quadrupole coupling constants of the He_N–OCS clusters increase with increasing N towards the value of free $OC^{33}S$ [$\chi = -29.112(3)$ MHz] [177]: He–OCS [$\chi_{aa} = -23.931(1)$ MHz]; He_2–OCS [$\chi_{aa} = -26.934(3)$ MHz]; He_3–OCS [$\chi_{aa} = -27.904(4)$ MHz]; He_4–OCS [$\chi_{aa} = -28.245(3)$ MHz]. This trend is a consequence of an increased alignment of the OCS axis with the *a*-inertial axis of the clusters with increasing N, under the assumption that the field gradient at the ^{33}S nucleus is not affected by the nearby helium atoms. The increased alignment is an indication of a more symmetric helium density around the OCS molecule at larger N values. The intermolecular vibrations of the OCS unit within the clusters probably play a minor role since the large amplitude motions are expected to be mainly restricted to the helium atoms because of the large relative mass of OCS. The extensive isotopic data for He_3–OCS were used to determine the locations of the helium atoms which were found to be around the equator of OCS at angles and distances similar to those of He–OCS. The almost constant blueshift of the infrared band origin in going from $N = 0$ to $N = 3$ in He_N–OCS confirms this geometry [134]. The three helium atoms are most likely not symmetrically distributed around the OCS molecule, contrary to the case of the (rare gas)–(rare gas)$'_3$ clusters which are clearly symmetric tops [89]. In such cases there will be a tunnelling barrier at the C_{3v} configuration; however, no excited state transitions were detected so far because of the low temperatures in the high pressure molecular expansion.

A further He–molecule system of interest is He–N_2O. The ro-vibrational spectrum of N_2O embedded in a helium nanodroplet has been observed by Nauta and Miller [178].

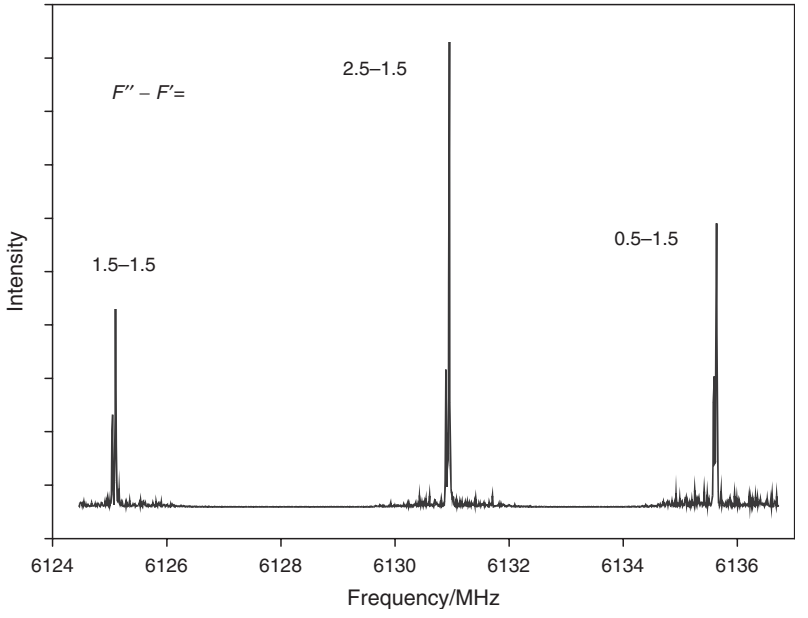

Figure 17. $J_K = 1_0$–0_0 transition of He_3–$OC^{33}S$ [28]. Note that the hyperfine splitting increases from He_2–OCS and approaches the splitting in the free OCS monomer. This is indication of an increased alignment of the OCS axis with the *a*-inertial axes of the clusters.

The mid-infrared spectrum of He–N_2O has been observed and analysed by Tang and McKellar [154] and three *ab initio* potential energy surfaces have been reported [7, 179, 180]. Our measurement of the microwave spectrum of He–N_2O [7] was based on predictions from the infrared work. Because of the low mass of the complex, only four transitions, namely $J_{K_a,K_c} = 1_{1,1}$–$0_{0,0}$; $1_{0,1}$–$0_{0,0}$; $1_{1,0}$–$1_{0,1}$; $1_{1,0}$–$1_{1,1}$, fall into the frequency range of our spectrometer and were measured. These four transitions form a closed loop which confirmed the assignment, together with double resonance experiments. For the normal isotopomers, the two ^{14}N nuclei result in complex nuclear quadrupole hyperfine structure for the rotational transitions. The spectra of three further isotopomers, He–$^{14}N^{15}NO$, He–$^{15}N^{14}NO$, and He–$^{15}N_2O$, were measured and assigned. In an effort to provide a potential energy surface of spectroscopic accuracy, we calculated the interaction energy at the CCSD(T) level of theory using the MOLPRO software package [181]. The aug-cc-pVTZ basis set was used for all atoms, supplemented with bond functions (3s, 3p, 2d, 1f, 1g), placed at the mid-point of the van der Waals bond [182]. The supermolecule approach was used and the basis set superposition error was accounted for by applying the full counterpoise correction [84]. The surface is characterized by a global minimum for an approximately T-shaped geometry (van der Waals distance $R = 2.979$ Å, angle θ between N_2O axis and $R = 87.4°$, interaction energy $V = -60.61\,cm^{-1}$), a local minimum at the oxygen end ($R = 4.111$ Å, $\theta = 0°$, $V = -33.10\,cm^{-1}$), and a very shallow minimum at the nitrogen end ($R = 4.534$ Å, $\theta = 180°$, $V = -21.44\,cm^{-1}$). A contour plot of the surface is given in figure 18. The quality of the potential energy surface was assessed by comparing

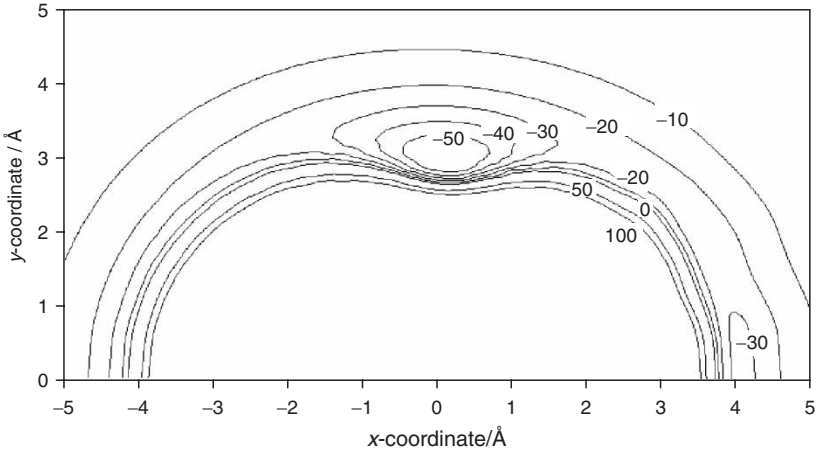

Figure 18. *Ab initio* potential energy surface of He–N_2O determined at the CCSD(T) level of theory [7]. The global minimum occurs at a near T-shape configuration at an energy of $-60.61\,cm^{-1}$. There is a local minimum is at the oxygen end ($-33.10\,cm^{-1}$), and a very shallow minimum at the nitrogen end ($-21.44\,cm^{-1}$). The zero-point energy level was determined from bound state calculations to be at $-21.35\,cm^{-1}$.

the experimental microwave transition frequencies and combination differences from the infrared data with those from bound state calculations [7]. For this purpose the surface was interpolated and the energies of rotational and ro-vibrational levels calculated. For the four microwave transitions, the deviations between experiment and calculation are less than 1.2%; if the mid-infrared combination differences are considered, the deviations are 3% at most, and less than 1% for most of the lines. This surface is thus of almost spectroscopic accuracy and has been used in quantum Monte Carlo calculations of N_2O solvated in small helium clusters [183].

The search and assignment of transitions of He_2–N_2O and He_3–N_2O followed similar procedures as outlined above for the OCS analogues. However, since N_2O is much lighter than OCS, the orientation of the N_2O unit within the cluster inertial axis system changes. He_2–N_2O is an asymmetric top molecule and the N_2O unit is aligned roughly along the *b*-inertial axis. The spectrum is thus dominated by *b*-type transitions which compounds the difficulties in the search and assignment procedure. Ultimately, two transitions, $J_{K_a,K_c} = 1_{1,1}$–$0_{0,0}$ and $2_{0,2}$–$1_{1,1}$ were found for the normal and the He_2–$^{15}N_2O$ isotopomers. The assignment was confirmed with double resonance experiments. For the singly ^{15}N substituted isotopomers, only the $J_{K_a,K_c} = 1_{1,1}$–$0_{0,0}$ transition was found. He_3–N_2O is an oblate quasi-symmetric top, and the N_2O unit lies roughly along the *c*-axis. Two transitions, namely $J_{K_a,K_c} = 1_{1,0}$–$0_{0,0}$ and $2_{2,0}$–$1_{1,0}$ were measured for four isotopomers. The respective alignments of N_2O in the inertial axis systems of the He_2–N_2O and He_3–N_2O clusters are confirmed by the analyses of the ^{14}N nuclear quadrupole hyperfine structures.

The He_2–molecule trimers are not very suitable systems for extraction of three-body non-additive interactions. Some of the reasons are: (i) the low polarizability of helium which leads, for example, to only a small exchange quadrupole moment

on the He_2 unit; (ii) the very large amplitude motions which makes modelling of the trimers difficult (see the work on He_2–N_2O by the groups of Carrington and McKellar [184]); (iii) the possibility of quantum effects involving the light helium atoms. However, characterization of the $He_{1,2}$–molecule complexes provide an important stepping stone for the investigation of larger He_N–molecule clusters. In this sense these systems lay the foundation for systematic helium solvation studies that shed light on the transition from the isolated molecule to the bulk quantum system [133, 135].

4. Summary

High resolution spectroscopic methods, such as pulsed molecular beam Fourier transform microwave spectroscopy, are ideal for the study of weakly bound complexes. In particular, it is possible to analyse the spectra of clusters of specific sizes individually although clusters of various sizes are produced simultaneously in the molecular expansion. This is achieved by a complex assignment procedure that needs not only to identify the quantum numbers of an observed transition, but also its molecular carrier. This procedure may involve, for example, the investigation of several isotopomers, sample pressure dependence studies of the signal intensities, and help from the corresponding mid-infrared investigations. The measured energy level differences, as well as number of spectroscopic parameters that can be obtained from the spectra, such as rotational, centrifugal distortion, and nuclear quadrupole coupling constants, and dipole moments, can be used to first test and then to improve the dimer potentials to spectroscopic accuracy. Indications for the presence of three-body non-additive contributions were found in the spectra of the mixed rare gas trimers and other ternary systems. The high resolution capability of the method of Fourier transform microwave spectroscopy makes it possible to resolve the sometimes very narrow nuclear quadrupole hyperfine structure in rotational transitions of the weakly bound complexes. The resulting nuclear quadrupole coupling constants provide information about both their structure and their internal dynamics. This information was utilized to monitor the change in internal rotation and inversion tunnelling dynamics in $(\text{rare gas})_{1,2,3}$–ammonia clusters. The studies on the $He_{1,2,3}$–molecule clusters represent a new direction in cluster research in that they provide a stepping stone for the investigation of new phenomena, such as quantum solvation, in much larger He_N–molecule clusters.

Acknowledgements

This work was funded by the Natural Sciences and Engineering Research Council of Canada. We thank D. Bremm, W. Topic, and Q. Wen for discussions and help with the manuscript.

References

[1] G. C. Maitland, M. Rigby, E. B. Smith, and W. A. Wakeham, *Intermolecular Forces, Their Origin and Determination* (Clarendon, Oxford, 1981).
[2] K. R. Leopold, G. T. Fraser, S. E. Novick, and W. Klemperer, Chem. Rev. **94,** 1807 (1994).
[3] S. Novick, Bibliography of Rotational Spectra of Weakly Bound Complexes, http://www.wesleyan.edu/chem/faculty/novick/vdw.html
[4] F.-M. Tao, Int. Rev. Phys. Chem. **20,** 617 (2001).
[5] J. M. Hutson, BOUND computer code, Ver. 4, distributed by Collaborative Computational Project No. 6 of the Science and Engineering Research Council, UK (1991).
[6] J. M. Hutson, Comp. Phys. Commun. **84,** 1 (1994).
[7] X. Song, Y. Xu, P. N. Roy, and W. Jäger, J. Chem. Phys. **121,** 12308 (2004).
[8] K. Harada, K. Tanaka, T. Tanaka, S. Nanbu, and M. Aoyagi, J. Chem. Phys. **117,** 7041 (2002).
[9] I. N. Kozin, M. M. Law, J. Tennyson, and J. M. Hutson, Comp. Phys. Commun. **163,** 117 (2004).
[10] P. E. S. Wormer and A. van der Avoird, Chem. Rev. **100,** 4109 (2000).
[11] M. Meuwly and J. M. Hutson, J. Chem. Phys. **110,** 8338 (1999).
[12] J. M. Bowman and S. S. Xantheas, Pure Appl. Chem. **76,** 29 (2004).
[13] J. A. Barker, in *Rare Gas Solids*, edited by M. L. Klein and J. A. Venables (Academic, London, 1976), p. 212.
[14] B. M. Axilrod and E. Teller, J. Chem. Phys. **11,** 299 (1943).
[15] E. Arunan, S. Dev, and P. K. Mandal, Appl. Spectrosc. Rev. **39,** 131 (2004).
[16] A. Ernesti and J. M. Hutson, J. Chem. Phys. **106,** 6288 (1997).
[17] J. M. Hutson, S. Liu, J. W. Moskowitz, and Z. Bai, J. Chem. Phys. **111,** 8378 (1999).
[18] T. J. Balle and W. H. Flygare, Rev. Sci. Instrum. **52,** 33 (1981).
[19] F. J. Lovas and R. D. Suenram, J. Chem. Phys. **87,** 2010 (1987).
[20] C. Chuang, C. J. Hawley, T. Emilsson, and H. S. Gutowsky, Rev. Sci. Instrum. **61,** 1629 (1990).
[21] U. Andresen, H. Dreizler, J.-U. Grabow, and W. Stahl, Rev. Sci. Instrum. **61,** 3694 (1990).
[22] Y. Xu and W. Jäger, J. Chem. Phys. **106,** 7968 (1997).
[23] J.-U. Grabow and W. Stahl, Z. Naturforsch. **45,** 1043 (1990).
[24] J. C. McGurc, T. G. Schmalz, and W. H. Flygare, Adv. Chem. Phys. **25,** 1 (1974).
[25] T. G. Schmalz and W. H. Flygare, in *Laser and Coherence Spectroscopy*, edited by J. I. Steinfeld (Plenum Press, New York, 1978), pp. 125–180.
[26] R. L. Shoemaker, *Laser and Coherence Spectroscopy* (Plenum Press, New York, 1978), p. 214.
[27] V. N. Markov, Y. Xu, and W. Jäger, Rev. Sci. Instrum. **69,** 4061 (1998).
[28] Y. Xu and W. Jäger, J. Chem. Phys. **119,** 5457 (2003).
[29] H. Darmawan, C. Tanjaroon, and W. Jäger (to be published).
[30] H. S. Gutowsky, T. D. Klots, C. Chuang, C. A. Schmuttenmaer, and T. Emilsson, J. Chem. Phys. **86,** 569 (1987).
[31] T. D. Klots, C. Chuang, R. S. Ruoff, T. Emilsson, and H. S. Gutowsky, J. Chem. Phys. **86,** 5315 (1987).
[32] H. S. Gutowsky, T. D. Klots, and C. E. Dykstra, J. Chem. Phys. **93,** 6216 (1990).
[33] E. Arunan, C. E. Dykstra, T. Emilsson, and H. S. Gutowsky, J. Chem. Phys. **105,** 8495 (1996).
[34] Y. Xu, M. C. L. Gerry, J. P. Connelly, and B. J. Howard, J. Chem. Phys. **98,** 2735 (1993).
[35] Y. Xu and W. Jäger, Phys. Chem. Chem. Phys. **2,** 3549 (2000).
[36] Y. Xu, W. Jäger, and M. C. L. Gerry, J. Mol. Spectrosc. **157,** 132 (1993).
[37] M. S. Ngari and W. Jäger, J. Chem. Phys. **111,** 3919 (1999).
[38] Z. Kisiel, B. A. Pietrewicz, and L. Pszcólkowski, J. Chem. Phys. **117,** 8248 (2002).
[39] M. S. Ngari and W. Jäger, Mol. Phys. **99,** 13 (2001).
[40] Y. Xu, G. S. Armstrong, and W. Jäger, J. Chem. Phys. **110,** 4354 (1998).
[41] Y. Xu and W. Jäger, Mol. Phys. **93,** 727 (1998).
[42] Z. Kisiel, E. Bialkowska-Jaworska, L. Pszczólkowski, A. Milet, C. Struniewicz, R. Moszynski, and J. Sadlej, J. Chem. Phys. **112,** 5767 (2000).
[43] Z. Kisiel, B. A. Pietrewicz, O. Desyatnyk, L. Pszczólkowski, I. Struniewicz, and J. Sadlej, J. Chem. Phys. **119,** 5907 (2003).
[44] S. W. Hunt, K. J. Higgins, M. B. Craddock, C. S. Brauer, and K. R. Leopold, J. Am. Chem. Soc. **125,** 13850 (2003).
[45] R. S. Ruoff, T. Emilsson, C. Chuang, T. D. Klots, and H. S. Gutowsky, J. Chem. Phys. **90,** 4069 (1989).
[46] R. S. Ruoff, T. Emilsson, C. Chuang, T. D. Klots, and H. S. Gutowsky, J. Chem. Phys. **93,** 6363 (1990).
[47] H. S. Gutowsky, J. Chen, P. J. Hajduk, and R. S. Ruoff, J. Phys. Chem. **94,** 7774 (1990).

[48] H. S. Gutowsky, P. J. Hajduk, C. Chuang, and R. S. Ruoff, J. Chem. Phys. **92,** 862 (1990).
[49] D. L. Fiacco, S. W. Hunt, and K. R. Leopold, J. Phys. Chem. A **104,** 8323 (2000).
[50] K. I. Peterson, R. D. Suenram, and F. J. Lovas, J. Chem. Phys. **94,** 106 (1991).
[51] K. I. Peterson, R. D. Suenram, and F. J. Lovas, J. Chem. Phys. **90,** 5964 (1989).
[52] D. Priem, T.-K. Ha, and A. Bauder, J. Chem. Phys. **113,** 169 (2000).
[53] S. A. Peebles and R. L. Kuczkowski, J. Chem. Phys. **109,** 5276 (1998).
[54] S. A. Peebles and R. L. Kuczkowski, J. Phys. Chem. A **102,** 8091 (1998).
[55] R. A. Peebles, S. A. Peebles and R. L. Kuczkowski, Mol. Phys. **96,** 1355 (1999).
[56] S. A. Peebles and R. L. Kuczkowski, J. Chem. Phys. **111,** 10511 (1999).
[57] R. A. Peebles and R. L. Kuczkowski, J. Chem. Phys. **112,** 8839 (2000).
[58] E. Arunan, T. Emilsson, and H. S. Gutowsky, J. Chem. Phys. **116,** 4886 (2002).
[59] E. Arunan, T. Emilsson, and H. S. Gutowsky, J. Am. Chem. Soc. **116,** 8418 (1994).
[60] H. S. Gutowsky, E. Arunan, T. Emilsson, S. L. Tschopp, and C. E. Dykstra, J. Chem. Phys. **103,** 3917 (1995).
[61] H. S. Gutowsky, T. D. Klots, C. Chuang, J. D. Keen, C. A. Schmuttenmaer, and T. Emilsson, J. Am. Chem. Soc. **109,** 5633 (1987).
[62] E. Arunan, T. Emilsson, H. S. Gutowsky, and C. E. Dykstra, J. Chem. Phys. **114,** 1242 (2001).
[63] W. Jäger, Y. Xu, and M. C. L. Gerry, J. Chem. Phys. **99,** 919 (1993).
[64] Y. Xu, W. Jäger, J. Djauhari, and M. C. L. Gerry, J. Chem. Phys. **103,** 2827 (1995).
[65] J.-U. Grabow, A. S. Pine, G. T. Fraser, F. J. Lovas, R. D. Suenram, T. Emilsson, E. Arunan and H. S. Gutowsky, J. Chem. Phys. **102,** 1181 (1995).
[66] M. Keil, L. J. Danielson, and P. J. Dunlop, J. Chem. Phys. **94,** 296 (1991).
[67] D. A. Barrow and R. A. Aziz, J. Chem. Phys. **89,** 6189 (1988)
[68] D. A. Barrow, M. J. Slaman, and R. A. Aziz, J. Chem. Phys. **91,** 6348 (1989); **96,** 5555 (E) (1992).
[69] R. A. Aziz and A. van Dalen, J. Chem. Phys. **78,** 2413 (1983).
[70] R. A. Aziz and A. van Dalen, J. Chem. Phys. **78,** 2402 (1983).
[71] S. M. Cybulski and R. R. Toczyłowski, J. Chem. Phys. **111,** 10520 (1999).
[72] J. L. Cacheiro, B. Fernández, D. Marchesan, S. Coriani, C. Hättig, and A. Rizzo, Mol. Phys. **102,** 101 (2004).
[73] S. M. Cybulski and R. R. Toczyłowski, J. Chem. Phys. **119,** 5487 (2003).
[74] K. T. Tang and J. P. Toennies, J. Chem. Phys. **118,** 4976 (2003).
[75] R. J. Le Roy, LEVEL 7.5: A Computer Program for Solving the Radial Schrödinger Equation for Bound and Quasibound Levels, University of Waterloo Chemical Physics Research report CP-655 (2002). The source code and manual for this program may be obtained from the 'Computer Programs' link on the www site http://leroy.uwaterloo.ca
[76] J. M. Steed, T. A. Dixon, and W. Klemperer, J. Chem. Phys. **70,** 4095 (1979).
[77] E. Bar-Ziv and S. Weiss, J. Chem. Phys. **64,** 2417 (1976).
[78] G. Birnbaum, M. Krauss, and L. Frommhold, J. Chem. Phys. **80,** 2669 (1984).
[79] M. Krauss and B. Guillot, Chem. Phys. Lett. **158,** 142 (1989).
[80] D. Bremm and W. Jäger (to be published).
[81] K. Hald, A. Halkier, P. Jørgensen, S. Coriani, C. Hättig, and T. Helgaker, J. Chem. Phys. **118,** 2985 (2003).
[82] D. E. Woon, and T. H. Dunning, J. Chem. Phys. **100,** 2975 (1993).
[83] H.-J. Werner, P. J. Knowles, M. Schütz, R. Lindh, P. Celani, T. Korona, G. Rauhut, F. R. Manby, R. D. Amos, A. Bernhardsson, A. Berning, D. L. Cooper, M. J. O. Deegan, A. J. Dobbyn, F. Eckert, C. Hampel, G. Hetzer, A. W. Lloyd, S. J. McNicholas, W. Meyer, M. E. Mura, A. Nicklaß, P. Palmieri, R. Pitzer, U. Schumann, H. Stoll, A. J. Stone R. Tarroni, and T. Thorsteinsson, MOLPRO, version 2002.6, a package of *ab initio* programs, 2003, see http://www.molpro.net
[84] S. Boys and F. Bernadi, Mol. Phys. **19,** 553 (1970).
[85] F. B. van Duijneveldt, J. G. C. M. van Duijneveldt-van de Rijdt, and J. H. van Lenthe, Chem. Rev. **94,** 1873 (1994).
[86] E. J. Campbell, L. W. Buxton, and A. C. Legon, J. Chem. Phys. **78,** 3483 (1983).
[87] P. R. Bunker, J. Mol. Spectrosc. **46,** 119 (1973).
[88] Y. Xu, W. Jäger, and M. C. L. Gerry, J. Chem. Phys. **100,** 4171 (1993).
[89] Y. Xu and W. Jäger, J. Chem. Phys. **107,** 4788 (1997).
[90] A. R. Cooper, S. Jain, and J. M. Hutson, J. Chem. Phys. **98,** 2160 (1993).
[91] A. Ernesti and J. M. Hutson, J. Chem. Phys. **103,** 3386 (1995).
[92] R. A. Aziz and M. J. Slaman, Chem. Phys. **130,** 187 (1989).
[93] B. Gulliot, R. D. Mountain, and G. Birnbaum, J. Chem. Phys. **90,** 650 (1989).
[94] B. Gulliot, J. Chem. Phys. **91,** 3456 (1989).
[95] J. Jellinek (Editor), *Theory of Atomic and Molecular Clusters* (Springer Verlag, Berlin, 1999).

[96] P. Bunker and P. Jensen, *Molecular Symmetry and Spectroscopy*, 2nd ed. (NRC Research Press, Ottwa, 1998).
[97] G. T. Fraser, D. D. Nelson Jr., A. Charo, and W. Klemperer, J. Chem. Phys. **82,** 2535 (1985).
[98] D. D. Nelson Jr., G. T. Fraser, K. I. Peterson, K. Zhao, W. Klemperer, F. J. Lovas, and R. D. Suenram, J. Chem. Phys. **85,** 5512 (1986).
[99] E. Zwart, H. Linnartz, W. L. Meerts, G. T. Fraser, D. D. Nelson Jr., and W. Klemperer, J. Chem. Phys. **95,** 793 (1991).
[100] E. Zwart and W. L. Meerts, Chem. Phys. **151,** 407 (1991).
[101] D. G. Melnik, S. Gopalakrishnan, T. A. Miller, F. C. De Lucia, and S. Belov, J. Chem. Phys. **114,** 6100 (2001).
[102] D. G. Melnik, T. A. Millar, and F. C. De Lucia, J. Mol. Spectrosc. **214,** 202 (2002).
[103] G. Chałasiński, S. M. Cybulski, M. M. Szczęśniak, and S. Scheiner, J. Chem. Phys. **91,** 7809 (1989).
[104] M. Bulski, P. E. S. Wormer, and A. van der Avoird, J. Chem. Phys. **94,** 491 (1991).
[105] J. W. I. van Bladel, A. van der Avoird, and P. E. S. Wormer, J. Chem. Phys. **94,** 501 (1991).
[106] J. W. I. van Bladel, A. van der Avoird, and P. E. S. Wormer, J. Phys. Chem. **95,** 5414 (1991).
[107] J. W. I. van Bladel, A. van der Avoird, and P. E. S. Wormer, Chem. Phys. **165,** 47 (1992).
[108] G. C. M. van der Sanden, P. E. S. Wormer, A. van der Avoird, J. Schleipen, and J. J. ter Meulen, J. Chem. Phys. **97,** 6460 (1992); **100,** 5393 (1994) (E).
[109] F.-M. Tao and W. Klemperer, J. Chem. Phys. **101,** 1129 (1994).
[110] J. Millan, N. Halberstadt, G. van der Sanden, and A. van der Avoird, J. Chem. Phys. **106,** 9141 (1997).
[111] C. A. Schmuttenmaer, R. C. Cohen, and R. J. Saykally, J. Chem. Phys. **101,** 146 (1994).
[112] D. H. Gwo, M. Havenith, K. L. Busarow, R. C. Cohen, C. A. Schmuttenmaer, and R. J. Saykally, Mol. Phys. **71,** 453 (1990).
[113] C. A. Schmuttenmaer, R. C. Cohen, J. G. Loeser, and R. J. Saykally, J. Chem. Phys. **95,** 9 (1991).
[114] C. A. Schmuttenmaer, J. G. Loeser, and R. J. Saykally, J. Chem. Phys. **101,** 139 (1994).
[115] J. van Wijngaarden and W. Jäger, J. Chem. Phys. **115,** 6504 (2001).
[116] J. van Wijngaarden and W. Jäger, Chem. Phys. **283,** 29 (2002).
[117] J. van Wijngaarden and W. Jäger, J. Am. Chem. Soc. **125,** 14631 (2003).
[118] J. van Wijngaarden and W. Jäger, Phys. Chem. Chem. Phys. **4,** 4883 (2002).
[119] J. van Wijngaarden and W. Jäger, J. Chem. Phys. **116,** 2379 (2002).
[120] J. van Wijngaarden and W. Jäger, Mol. Phys. **99,** 1215 (2001).
[121] J. van Wijngaarden and W. Jäger, J. Chem. Phys. **114,** 3968 (2001).
[122] W. Gordy and R. L. Cook, *Microwave Molecular Spectra*, 3rd ed. (Wiley, New York, 1984).
[123] M. D. Marshall and J. S. Muenter, J. Mol. Spectrosc. **85,** 322 (1981).
[124] L. Abouaf-Marguin, M. E. Jacox, and D. E. Milligan, J. Mol. Spectrosc. **67,** 34 (1977).
[125] C. H. Townes and A. L. Schawlow, *Microwave Spectroscopy* (Dover, New York, 1975), p. 306.
[126] M. T. Weiss and M. W. P. Strandberg, Phys. Rev. **83,** 567 (1951).
[127] M. E. Jacox and W. E. Thompson, J. Mol. Spectrosc. **228,** 414 (2004).
[128] S. Goyal, D. L. Schutt, and G. Scoles, Phys. Rev. Lett. **69,** 933 (1992).
[129] S. Goyal, D. L. Schutt, and G. Scoles, J. Phys. Chem. **97,** 2236 (1993).
[130] R. Fröchtenicht, J. P. Toenies, and A. F. Vilesov, Chem. Phys. Lett. **229,** 1 (1994).
[131] S. Grebenev, J. P. Toennies, and A. F. Vilesov, Science **279,** 2083 (1998).
[132] K. Nauta, D. T. Moore, P. L. Stiles, and R. E. Miller, Science **292,** 481 (2001).
[133] J. Tang, Y. Xu, A. R. W. McKellar, and W. Jäger, Science **297,** 2030 (2002).
[134] J. Tang and A. R. W. McKellar, J. Chem. Phys. **119,** 5467 (2003).
[135] Y. Xu, W. Jäger, J. Tang, and A. R. W. McKellar, Phys. Rev. Lett. **91,** 163401 (2003).
[136] J. Tang and A. R. W. McKellar, J. Chem. Phys. **121,** 181 (2004).
[137] J. Tang, A. R. W. McKellar, F. Mezzacapo, and S. Moroni, Phys. Rev. Lett. **92,** 145503 (2004).
[138] J. Tang and A. R. W. McKellar, J. Chem. Phys. **119,** 754 (2003).
[139] A. R. W. McKellar, J. Chem. Phys. **121,** 6868 (2004).
[140] Y, Xu and W. Jäger, 59th International Symposium on Molecular Spectroscopy, Columbus, Ohio, paper TH10, June 2004.
[141] Y. Kwon, P. Huang, M. V. Patel, D. Blume, and K. B. Whaley, J. Chem. Phys. **113,** 6469 (2000).
[142] F. Paesani, F. A. Gianturco, and K. B. Whaley, J. Chem. Phys. **115,** 10225 (2001).
[143] S. Moroni, A. Sarsa, S. Fantoni, K. Schmidt, and S. Baroni, Phys. Rev. Lett. **90,** 143401 (2003).
[144] F. Paesani and K. B. Whaley, J. Chem. Phys. **121,** 4180 (2004).
[145] N. Blinov, X. Song, and P. N. Roy, J. Chem. Phys. **120,** 5916 (2004).
[146] S. Moroni, N. Blinov, and P.-N. Roy, J. Chem. Phys. **121,** 3577 (2004).
[147] F. Paesani and K. B. Whaley, J. Chem. Phys. **121,** 5293 (2004).
[148] S. Drucker, F.-M. Tao, and W. Klemperer, J. Phys. Chem. **99,** 2646 (1995).
[149] K. Higgins, F.-M. Tao, and W. Klemperer, J. Chem. Phys. **109,** 3048 (1998).

[150] K. Higgins and W. Klemperer, J. Chem. Phys. **110,** 1383 (1999).
[151] M. J. Weida, J. M. Sperhac, D. J. Nesbitt, and J. M. Hutson, J. Chem. Phys. **101,** 8351 (1994).
[152] A. R. W. McKellar, Y. Xu, W. Jäger, and C. Bissonette, J. Chem. Phys. **110,** 10766 (1999).
[153] J. Tang and A. R. W. McKellar, J. Chem. Phys. **115,** 3053 (2001).
[154] J. Tang and A. R. W. McKellar, J. Chem. Phys. **117,** 2586 (2002).
[155] Y. Xu and W. Jäger, J. Mol. Struct. **599,** 211 (2001).
[156] W. Topic and W. Jäger, J. Chem. Phys. (in press).
[157] S. Grebenev, M. Hartmann, M. Havenith, B. Sartakov, J. P. Toennies, and A. F. Vilesov, J. Chem. Phys. **112,** 4485 (2000).
[158] S. Grebenev, J. P. Toennies, and A. F. Vilesov, Science **279,** 2083 (2000).
[159] J. M. M. Howson and J. M. Hutson, J. Chem. Phys. **115,** 5059 (2001).
[160] Y. Xu and W. Jäger (unpublished results).
[161] W. Jäger, Y. Xu, G. Armstrong, M. C. L. Gerry, F. Y. Naumkin, F. Wang, and F. R. W. McCourt, J. Chem. Phys. **109,** 5420 (1998).
[162] W. Jäger and M. C. L. Gerry, Chem. Phys. Lett. **196,** 274 (1992).
[163] W. Jäger, M. C. L. Gerry, C. Bissonnette, and F. R. W. McCourt, Faraday Discuss. **97,** 105 (1994).
[164] W. Jäger, Y. Xu, N. Heineking, and M. C. L. Gerry, J. Chem. Phys. **99,** 7510 (1993).
[165] Q. Wen and W. Jäger, J. Chem. Phys. **122,** 214310 (2005).
[166] A. Ernesti and J. M. Hutson, J. Chem. Phys. **101,** 5438 (1994).
[167] J. M. Hutson, Mol. Phys. **84,** 185 (1995).
[168] K. M. Atkins and J. M. Hutson, J. Chem. Phys. **105,** 440 (1996).
[169] K. Harada, K. Tanaka, T. Tanaka, S. Nanbu, and M. Aoyagi, J. Chem. Phys. **117,** 7041 (2002).
[170] Y. Liu, W. Jäger, and P. N. Roy (unpublished results).
[171] Y. Xu, Y. Liu, P. N. Roy, and W. Jäger (unpublished results).
[172] H. Darmawan and W. Jäger (unpublished results).
[173] K. Tanaka, H. Ito, K. Harada, and T. Tanaka, J. Chem. Phys. **80,** 5893 (1984).
[174] A. M. Andrews, L. Nemes, S. L. Maruca, K. W. Hillig II, R. L. Kuczkowski, and J. S. Muenter, J. Mol. Spectrosc. **160,** 422 (1993).
[175] Y. Xu and W. Jäger, Chem. Phys. Lett. **350,** 417 (2001).
[176] B. C. Dian, K. O. Douglass, G. G. Brown, S. Geyer, and B. H. Pate, 60th Ohio State University International Symposium on Molecular Spectroscopy, June 20–24, 2005, paper TA06.
[177] I. Merke and H. Dreizler, Z. Naturforsch., A: Phys. Sci. **42,** 1043 (1987).
[178] K. Nauta and R. E. Miller, J. Chem. Phys. **115,** 10254 (2001).
[179] B. Chang, O. Akin-Ojo, R. Bukowski, and K. Salewicz, J. Chem. Phys. **119,** 11654 (2003).
[180] Y. Zhou and D. Xie, J. Chem. Phys. **120,** 8575 (2004).
[181] C. Angeli, K. L. Bak, V. Bakken, O. Christiansen, R. Cimiraglia, S. Coriani, P. Dahle, E. K. Dalskov, T. Enevoldsen, B. Fernandez, C. Hättig, K. Hald, A. Halkier, H. Heiberg, T. Helgaker, H. Hettema, H. J. Aagaard Jensen, D. Jonsson, P. Jørgensen, S. Kirpekar, W. Klopper, R. Kobayashi, H. Koch, A. Ligabue, O. B. Lutnæs, K. V. Mikkelsen, P. Norman, J. Olsen, M. J. Packer, T. B. Pedersen, Z. Rinkevicius, E. Rudberg, T. A. Ruden, K. Ruud, P. Salek, A. Sanchez de Meras, T. Saue, S. P. A. Sauer, B. Schimmelpfennig, K. O. Sylvester-Hvid, P. R. Taylor, O. Vahtras, D. J. Wilson, and H. Ågren, DALTON, a molecular electronic structure program, Release 2.0 (2005), see http://www.kjemi.uio.no/software/dalton/dalton.html
[182] F.-M. Tao and Y. Pan, Mol. Phys. **81,** 507 (1994).
[183] S. Moroni, N. Blinov, and P. N. Roy, J. Chem. Phys. **121,** 3577 (2004).
[184] X.-G. Wong, T. Carrington Jr., J. Tang, and A. R. W. McKellar, J. Chem. Phys. **123**, 034301 (2005).